Crystal mush growth and collapse on a steep wall: the Marginal Border Series of the Skaergaard Intrusion, East Greenland

Marian B. Holness[1], Madeleine C.S. Humphreys[2,7], Olivier Namur[3], Jens C.Ø. Andersen[4], Christian Tegner[5], and Troels F.D. Nielsen[6]

1. Department of Earth Sciences, University of Cambridge, Downing Street, Cambridge, CB2 3EQ, UK. marian@esc.cam.ac.uk

2. Department of Earth Sciences, University of Oxford, South Parks Road, Oxford, OX1 3AN, UK

3. Division of Geology, Katholieke Universiteit Leuven, Celestijnenlaan 200e – Box 2408, 3001 Leuven, Belgium

4. Camborne School of Mines, University of Exeter, Penryn Campus, Tremough, Penryn, TR10 9FE, UK

5. Department of Earth Sciences, Aarhus University, Høegh-Guldbergs Gade 2, DK-8000 Århus C, Denmark

6. Geological Survey of Denmark and Greenland, Øster Voldgade 10, DK-1350, Copenhagen, Denmark

7. Department of Earth Sciences, Durham University, Science Labs, Durham, DH1 3LE, UK

September 2021

ABSTRACT

The Skaergaard Intrusion of East Greenland solidified as a closed system, with the development of progressively more fractionated material at the roof, floor and vertical walls of the magma chamber. We argue, using field observations of the exposed western margin together with detailed microstructural and geochemical analysis, that the mush on the vertical walls of the Skaergaard Intrusion reached a maximum thickness of ~180m, and was highly unstable. Material was lost both continuously, due to non-retention of poorly consolidated material, and during episodic collapse events. The almost complete absence in the wall rocks of material formed in LZc times (following the saturation of the bulk magma in Fe-Ti oxides) was likely to have been caused by a collapse event, perhaps related to faulting of the actively extending Greenlandic margin. A second major collapse of the MBS occurred during the later stages of solidification, with the greatest loss of material occurring in a region of the wall with an unusually thick mush, creating a transient and localised increase in the thickness of the floor mush. This work demonstrates the importance of vertical walls in supplying loose, disaggregated material to form mobile magmatic slurries that may contribute to floor cumulates or be entrained and erupted in long-lived systems.

INTRODUCTION

There is much recent controversy concerning the extent of fractionation of mafic magmas in crustal chambers (Ashwal *et al*., 2005; Latypov, 2009; Marsh, 2013; Latypov *et al*., 2015; Yuan *et al*., 2017). Central to the question of how magma fractionates is the stability, structure and extent of the crystal mush that forms on the margins of bodies of magma stalled in the crust. Disaggregation of these mush zones could also supply material ('antecrysts') to erupted magma, and may be wrongly attributed to recharge and rejuvenation events. Although horizontal crystal mushes have been abundantly studied from a wide range of intrusions, the physical behaviour of mush zones forming on vertical surfaces is comparatively poorly understood.

The Skaergaard Intrusion of East Greenland is characterised by the sequential appearance of increasingly more evolved primocryst assemblages towards its central, and last-to-crystallise, regions (Wager & Deer, 1939; Wager & Brown, 1968; McBirney, 1989a). While much attention has been focussed on the floor cumulates, there has been little corresponding work on the material contemporaneously crystallised on its steeply-dipping walls (Wager & Deer, 1939, Wager & Brown, 1968; Hoover, 1989a, b; Humphreys & Holness, 2010; Namur *et al*., 2013) despite it comprising ~16 vol.% of the intrusion (Nielsen (2004) and its possible significance in contributing to fractionation. In this contribution, we report the results of a detailed microstructural and geochemical study of the Skaergaard wall, and show how mush thickness varied during solidification, linking this to loss of material either by a continuous rain of poorly consolidated grains and grain clusters, or to catastrophic collapse events triggered by earthquakes during crustal extension.

GEOLOGICAL SETTING

The Skaergaard Intrusion comprises a body (8 x 11 x 4km, Nielsen, 2004) of relatively evolved tholeiitic basalt that was injected into a fault-bounded (Irvine *et al*., 1998; Nielsen, 2004) space forming on the extending margin of East Greenland during the opening of the North Atlantic (Figure 1). The intrusion lies at the unconformity between Precambrian gneisses and a sequence of Cretaceous to Palaeogene sediments overlain by Palaeogene volcanic rocks (Wager & Deer, 1939). It was inflated to its final size by a series of magma pulses (Holness *et al.,* 2007a, b; 2015) before remaining closed during the rest of its solidification history. Coast-parallel flexure associated with the opening of the North Atlantic continued after solidification, tipping the intrusion ~20˚ to the south.

Solidification resulted in the formation of three different series (Wager & Deer, 1939): the (volumetrically dominant) Layered Series crystallised upwards from the floor; the Marginal Border Series (MBS) crystallised inwards from the walls: and the Upper Border Series (UBS) crystallised downwards from the roof, meeting the Layered Series at the Sandwich Horizon. Progressive fractionation within the chamber resulted in these three series displaying correlated changes in liquidus assemblage (Wager & Deer, 1939; Wager & Brown, 1968; McBirney, 1989a; Hoover, 1989a; Salmonsen & Tegner, 2013). The Layered Series is divided into Lower, Middle and Upper Zones (Figure 1) based on the absence of cumulus olivine in the Middle Zone, and is underlain by the Hidden Zone (HZ), which is ~150m thick in the region of the Uttental Plateau (Maaløe, 1976; Holness *et al*., 2007b; 2015). Lower Zone is subdivided: LZa contains cumulus olivine and plagioclase; the base of LZb is marked by the arrival of cumulus augite; and the base of LZc is marked by the arrival of cumulus Fe-Ti oxides. Upper Zone is also subdivided; the base of UZb defines the

arrival of cumulus apatite, while the base of UZc marks the first appearance of the mosaic form of ferro-hedenbergite inverted from β-ferrobustamite. The UBS (Naslund, 1984; Salmonsen & Tegner, 2013) and MBS (Hoover, 1989a) are similarly subdivided, with the equivalent MBS divisions denoted by an asterisk. There is no UZc* equivalent to UZc (Hoover, 1989a), most likely due to geometrical constraints in the almost completely solidified magma body. Troctolitic, anorthositic and gabbroic autoliths are common in the Layered Series, and are especially abundant from the middle of LZb through to the lower half of MZ. They are thought to be derived from collapse of the UBS (Irvine *et al*., 1998).

The thickness of each of the Layered Series subdivisions in the standard profile that Tegner *et al*. (2009) collected close to the centre of the intrusion is: LZa – 175m (325m when HZ is included); LZb – 555m; LZc – 160m; MZ – 270m; UZa – 455m; UZb – 430; and UZc – 120m. The thickness of each subdivision varies laterally: this variation is generally symmetrical, with the greatest thickness found in the centre of the chamber floor (Nielsen, 2004; Holness *et al*., 2017a). MZ and UZb are exceptions: in agreement with the stratigraphy presented by McBirney (1989a), detailed reconstructions of the internal geometry of the intrusion (Nielsen, 2004) suggest that these two subdivisions are asymmetrical, with the greatest thickness of both occurring closer to the western than the eastern margin.

The Marginal Border Series

The outer contact of the intrusion on much of the western margin follows pre-existing or syn-magmatic faults (Nielsen, 2004). It dips steeply into the intrusion (Wager & Deer, 1939; Figure 1), but is shallow (~25˚; Wager & Deer, 1939) where it crosses the unconformity on Mellemø: it is not known how far into the intrusion this region of shallow dip extends. The localised region of shallow dip, forming a kink in the geometry of the western contact, remains after restoration of the intrusion to its original orientation.

The MBS becomes thicker with increasing stratigraphic height on the intrusion walls, reaching a maximum at the level of the Sandwich Horizon (Hoover, 1989a): the greatest exposed thickness, on the Skaergaard Peninsula, is ~650m (Figures 1, 2). Each MBS subdivision first appears at structurally higher levels than its Layered Series equivalent (Figure 2), attributed by Hoover (1989a) to differences in the liquid composition between the walls and floor. On the western margin, this is most marked for LZc*, which is apparently absent altogether on the eastern margin (Hoover, 1989a). Although exposure is incomplete, there appears to be no difference in thickness between equivalent MBS subdivisions on the two sides of the intrusion.

The outermost MBS (LZa*) contains localised occurrences of ‘Wavy Pyroxene rock’ (Wager & Brown, 1968), characterised by abundant cm- to dm-scale lenses of relatively coarse-grained gabbro (Figure 3a). The lenses dip towards the intrusion margin, and show a systematic morphological evolution, increasing in size and spacing, and becoming more diffuse and irregular, away from the contact (Figure 3b). They are interpreted as late magmatic segregations formed by ductile tearing of partially consolidated mush, with the morphological evolution ascribed to the mush on the inner margin of the MBS becoming increasingly poorly consolidated as the MBS thickened (Humphreys & Holness, 2010).

First appearing in the inner parts of LZa* are steeply dipping to vertical modal banding, distinct from the graded modal layering of the Layered Series: bands are cm- to dm-thick, have a characteristic corrugated

morphology, with cuspate or colloform outlines on horizontal outcrop surfaces (Wager & Brown, 1968), and are finer-grained and more melanocratic than the uniform gabbro on either side (Figure 4a; Namur *et al.*, 2013). A morphological evolution occurs with increasing distance into the intrusion, with bands becoming progressively more deeply scalloped and fingered, towards an endpoint of discontinuous trough-like features elongated perpendicular to the intrusion wall (Figures 4b, c). The colloform bands are argued to have been produced by chemical disequilibrium resulting from the suction of primitive liquid from the main magma body into the crystal mush, driven by shrinkage during solidification (Namur *et al.*, 2013). Their morphological evolution is attributed to the increasing thickness of the wall mush.

On the Uttental Plateau (near the intrusion floor; Figure 1), and locally on Kraemer Ø, the outermost part of the MBS, at the contact with the country rock, contains abundant xenoliths of gneiss, basalt from the overlying plateau lavas and ultramafic igneous rock (Wager & Deer, 1939; Hoover, 1989a; Kays & McBirney, 1982; Kays *et al.*, 1981; Irvine *et al.*, 1998; Markl, 2005). The Kraemer Ø xenolith cluster lies immediately south of a bend in the contact formed by the intersection of three steeply dipping faults (Nielsen, 2004; Figures 1, 2).

At all levels in the intrusion, the boundary between the MBS and the Layered Series is generally gradational (McBirney & Nicolas, 1997), comprising a region of abundant small angular unconformities in the modal layering (Figure 5a). These characteristics, together with the relative enrichment in melanocratic mineral grains of the Layered Series within 100m or so of the MBS, is attributed to a complex sequence of deposition and erosion events linked to the flow of crystal-laden currents down the walls (Wager & Deer, 1939; Irvine, 1980; McBirney & Nicolas, 1997). This “cross-bedded belt” (Wager & Brown, 1968) also contains numerous localised syn-magmatic, listric shear zones and normal faults (Wager & Brown, 1968; McBirney & Nicolas, 1997), some of which can be traced along strike for many tens of metres, consistent with downhill slipping and disruption of discrete bodies of coherent material (e.g. Irvine, 1980; McBirney & Nicolas, 1997; Irvine *et al.*, 1998), due to localised over-steepening of the floor possibly caused by compaction (Irvine, 1980). This explanation is consistent with the layering of the outermost Layered Series being relatively steeply dipping in the cross-bedded belt, with the dip reducing over some tens of metres into the intrusion (Figure 6a). The gradual decrease in spacing and throw of the faults in the cross-bedded belt along much of the western wall means that it is not generally obvious where to place the inner edge of this zone. We placed it where the fault spacing attains more than a few metres.

Locally in UZ, the boundary between the MBS and the Layered Series is well-defined, and is marked by a surface dipping into the intrusion separating coarse-grained material containing steeply-dipping colloform banding from shallow-dipping, finer-grained, laminated gabbros (Figure 5b). On Ivnarmiut and the northern part of the Mini-Peninsula (Figure 1) where the adjoining Layered Series belongs to UZa, the boundary between the MBS and the gently onlapping, strongly modally-banded Layered Series (Figure 6a), is marked by a melanocratic zone a few tens of cm wide (Figure 6b). This zone truncates bowl-like colloform banding in the innermost MBS (Figure 6c).

DIHEDRAL ANGLES AS A RECORD OF COOLING HISTORY

Because the geometry of poly-phase three-grain junctions in most gabbros and dolerites is essentially unmodified from that created during solidification, dihedral angles formed between two plagioclase grains and one grain of augite preserve a record of crystallisation and cooling (Holness *et al*., 2012a). The median value of the dihedral angle population, Θ_{cpp}, is a function of cooling rate. The lowest values are observed in rapidly cooled dolerites in which three-grain junctions are characterized by planar augite–plagioclase grain boundaries with augite almost perfectly pseudomorphing the original melt-filled space. In more slowly-cooled dolerites and gabbros, the augite–plagioclase grain boundaries in the vicinity of three-grain junctions are curved, indicative of simultaneous growth of the plagioclase forming the walls of the pore in which the augite is growing. The increase in Θ_{cpp} is therefore achieved by a change in the relative rate of growth of the plagioclase pore walls and the infilling augite (Holness, 2015).

Θ_{cpp} varies symmetrically in unfractionated dolerite sills and dykes, with the highest values in the slowly-cooled centre (Holness *et al*., 2012b; Holness *et al*., 2017b). In layered intrusions, Θ_{cpp} maintains a constant value over great stretches of stratigraphy with step-wise changes in Θ_{cpp} associated with changes in the liquidus assemblage of the bulk magma (Holness *et al*., 2013). Θ_{cpp} increases when the number of phases in the liquidus assemblage increases, and decreases when the liquidus assemblage loses a phase, associated with changes in the relative contribution of the latent heat of crystallisation to the overall enthalpy budget of the magma as the slope of the liquidus in temperature-composition space changes (Morse, 2011; Holness *et al*., 2013; Holness, 2015). For the case of the Skaergaard magma, there is a step-wise increase in Θ_{cpp} corresponding to the arrival of liquidus augite (the LZa/b boundary), one at the arrival of liquidus Fe-Ti oxides (the LZb/c boundary) and a third corresponding to the arrival of liquidus apatite (the UZa/b boundary) (Figure 7a). The boundaries separating MZ from the underlying LZc and overlying UZa are not marked by a change in Θ_{cpp}, since the number of phases remains the same: olivine and orthopyroxene interchange.

In detail, the stratigraphic variation of Θ_{cpp} in the upper parts of the Skaergaard Layered Series depends on the amount of interstitial liquid retained in the cumulates (Holness *et al*., 2017a). In the central part of the floor, comprising strongly adcumulate rocks (Tegner *et al*., 2009), Θ_{cpp} drops to ~80˚ through UZa, with a large, highly localised, increase associated with apatite-in followed by a return to values of ~80˚ through UZb and UZc (Figure 7a). In contrast, Θ_{cpp} in the more orthocumulate rocks near the western wall, as sampled by drill core 90-10 (Figure 1), remains high through UZa, with a small, stratigraphically localised, increase associated with apatite-in: high angles are maintained for a few tens of metres before dropping to values typical of the underlying UZa (Figure 7b; Holness *et al*., 2017a). In a further departure from the pattern seen in the central part of the floor, values of ~80˚ are seen only in a few metres of UZb, before Θ_{cpp} increases again in the uppermost parts of the core (Figure 7b),

The relatively short stretch of stratigraphy over which Θ_{cpp} is maintained at the high values associated with apatite-in, in contrast to the extended stretches of elevated Θ_{cpp} associated with the arrival of liquidus augite and Fe-Ti oxides, is most likely a consequence of the relatively short crystallisation period over which the increase in fractional latent heat associated with the apatite-bearing liquidus assemblage can affect cooling (Namur *et al*., 2014). The low values of Θ_{cpp} on either side of the apatite-in spike in the central part of the floor are a consequence of the grain boundaries between (ferro-)augite and plagioclase being

planar, a feature typical of rapid cooling, despite their undoubtedly slow crystallisation rates. This characteristic microstructure led Holness (2015) to coin the term 'macro-dolerite' to describe the coarse-grained rocks in which it occurs: it is attributed to cessation of plagioclase growth during the final stages of solidification of the interstitial liquid (Holness *et al*., 2013) and is associated with the presence of abundant granophyre (Holness *et al*., 2017a). The macro-dolerite microstructure is developed at lower stratigraphic levels in rocks with relatively small amounts of retained interstitial liquid (e.g. the centre of the floor) compared to those with a more orthocumulate character (e.g. drill core 90-10): this may be because of the more effective fractionation of late-stage liquids in more adcumulate rocks, leading to crystallisation of granophyre instead of plagioclase (Holness *et al.,* 2017a). The three-grain junction geometry in macro-dolerites cannot be used as a speedometer for solidification.

The dihedral angle forms during the last stages of mush solidification, when only a few volume percent of interstitial liquid remains. Therefore, the step-wise changes in Θ_{cpp}, caused by the change in fractional latent heat associated with a change in the liquidus assemblage of the overlying bulk liquid, always occur stratigraphically below the first appearance (or disappearance) of the phase responsible: this offset can be used to constrain the thickness of the mush at that moment (Holness *et al*., 2017a; c). Holness *et al*. (2017a) used this method to show that the mush on much of the floor of the Skaergaard intrusion was a few metres thick at the moment the bulk liquid became saturated in apatite (i.e. the UZa/b boundary), but in the region near the western wall sampled by the drill core 90-10 (Figure 1), the mush was ~100m thick at the same moment (Figure 7b).

SAMPLE LOCATIONS

Nine sample traverses were taken across the MBS, with eight on the western margin and one on the eastern (Figures 1, 2). With three exceptions, each traverse begins at the contact (where exposed) and continues into the Layered Series. Of these exceptions, Traverses 6 and 7 end within the outermost parts of the MBS, and the other (Traverse 9, on the east side of the intrusion) is truncated before the inner margin of the MBS by the absence of exposure. A tape-measure was used to determine distances within 50m of the contact. For the remaining samples, distances were calculated from the GPS position. Critical regions of interest were sampled at 2m sample spacing. A further set of samples was collected from UZb westwards along strike from the collar of drill core 90-10 (Holness *et al*., 2017a; Nielsen *et al*., 2015), linking the top of this core to the corresponding point where MBS meets the Layered Series in Traverse 8 (Figure 1).

ANALYTICAL METHODS

Petrography

All samples were examined to determine the position of step-changes in Θ_{cpp}, with a sub-set subjected to detailed analysis. We parameterise the dihedral angle in each sample using the median value of a population of > 30 true 3D angles measured using a 4-axis Leitz Universal Stage mounted on a James Swift optical microscope, with a x32 long working distance objective. We use the median because it can be determined accurately from a far smaller population of measurements than that required to determine the mode (Riegger & Van Vlack, 1960), and is less sensitive than the mean to the presence of unusually

small or large values in systems in which there is a range of true angles (i.e. those with anisotropy of interfacial energies or an incomplete approach to textural equilibrium). We calculated the 95% confidence interval for the median using the nonparametric method of Stickels & Hücke (1964) that is independent of the distribution function describing the population. In two places, the grain size reached ~5mm, with correspondingly few three-grain junctions in any one thin section: data from several closely-spaced samples were combined to create one large population of measurements.

The volumetric proportion of granophyric intergrowths and ilmenite-rich intergrowths, in samples from UZ* and UZ, was estimated from thin sections using a point counter (with up to 1000 points per thin section). These two types of interstitial intergrowth represent crystallised pockets of conjugate immiscible Si-rich and Fe-rich liquids (Holness *et al.*, 2011; Keevil *et al.*, 2020).

Bulk rock and mineral composition

Fused glasses for bulk rock analysis were prepared and analysed following the procedure of Tegner *et al.* (2009) for samples from Traverses 2, 5 and 8, chosen to provide a representative view of the lower, central and upper parts of the MBS.

Major- and minor-element compositions of minerals in the sample dividing the MBS and Layered Series on Ivnarmiut were acquired from polished thin sections using a JEOL-8600 wavelength-dispersive electron microprobe in the Research Laboratory for Archaeology and the History of Art, School of Archaeology, University of Oxford. Analyses were conducted with a 15 kV, 15 nA beam defocused to 5 μm (plagioclase) or 10 μm (olivine and pyroxenes) and with major elements analysed for 30 seconds on peak and minor elements for 60 seconds on peak. Background counting times were half peak counting times. Mineral standards were used for primary calibration and mineral and anhydrous glasses were used as secondary standards to check the accuracy of the calibration. Five samples from Traverse 8 (Skaergaard Peninsula) were examined by Nielsen *et al.* (2015), who present bulk rock Cu concentrations and average plagioclase compositions calculated from the CIPW norm.

RESULTS

General petrographic characteristics of the Marginal Border Series

The MBS rocks are significantly coarser grained than their Layered Series counterparts, with the grain size in the outermost Layered Series decreasing significantly through the cross-bedded belt. In contrast to the predominantly euhedral primocrysts of the Layered Series, commonly with a shape-preferred orientation resulting in a fabric indicative of growth in a liquid-rich environment before accumulation and re-arrangement, those in the MBS are more anhedral, with no preferred orientation.

The LZa* rocks are the most plagioclase-rich of the MBS, with plagioclase mode decreasing steadily as the MBS gabbros become more evolved (c.f. Tegner *et al.*, 2009). Plagioclase-plagioclase grain boundaries are typical of those formed by *in situ* growth to impingement (e.g. Holness *et al.* 2019; 2020): they are only rarely parallel to growth faces of either or both of the two constituent grains; they are undulose and commonly interpenetrant (Figure 8a). Olivine primocrysts are generally anhedral, commonly with inclusions of plagioclase, indicative of significant overgrowth from interstitial liquid (Figure 8b). However,

olivine-rich samples contain more equant olivine, commonly forming clumps of grains joined on planar low index faces (Figure 8c). Clumps of facetted olivine grains are locally present through LZb*.

The arrival of primocryst clinopyroxene is marked by an increase in augite mode and progressive loss of poikilitic habit. Primocryst augite may be anhedral, with irregular outlines caused by overgrowth from the interstitial liquid (Figure 8d). However, augite primocrysts, particularly in augite-rich rocks, also form grains elongate along [001], with a simple twin boundary on (100) (Figure 8e). These grains are euhedral where enclosed by large grains of plagioclase (Figure 8e), but subhedral to anhedral where surrounded by material of comparable grain size. The (apparent) overall aspect ratio of these elongate twinned grains may reach ~15. The proportion of twinned relative to untwinned grains is variable, but can be significantly more than 50%. These twinned, elongate, euhedral augite grains are a common, but previously undocumented, feature of the Layered Series from LZb upwards, particularly in the central part of the floor.

There is very little LZc* on the western wall (see later), with the arrival of primocrystic Fe-Ti oxides generally associated with the loss of olivine primocrysts and thus marking the boundary between LZb* and MZ*. The sharp increase in oxide mode is associated with a change from anhedral to generally euhedral morphology, with octahedra of magnetite and elongate prisms of ilmenite (Figure 8f). Although MZ* (and MZ) is defined by the absence of abundant primocrystic olivine, a few vol.% of olivine is locally present in both MZ* and MZ (Wager & Brown, 1968): these olivine grains tend to be small, anhedral and enclosed by pyroxene. A polycrystalline olivine rim, analogous to those in the Layered Series (e.g. Holness *et al*., 2011), separates Fe-Ti oxides from any enclosing augite.

The MZ*/UZa* boundary is marked by the re-appearance of olivine primocrysts, which are commonly large and anhedral. The polycrystalline monomineralic clumps that are so common in LZ* are absent. Primocrystic apatite is particularly abundant at the outer margin of UZb* (visible in the field as a change of outcrop character to a rubbly brown, often Cu-stained, highly weathered rock).

Throughout the MBS, pockets of late-stage liquid containing granophyre commonly also include grains of apatite. Hydrous alteration concentrates around these pockets, suggestive of high H_2O content in these evolved liquids, released on solidification. From about half-way through MZ*, late-stage liquid pockets may also contain ilmenite-rich intergrowths (Figure 8g). The co-existence of granophyre and ilmenite-rich intergrowths, and the absence of any reactive symplectites, indicate only limited spatial separation of the two conjugate immiscible silicate liquids once the interstitial liquid encountered the binode (Holness *et al.,* 2011).

The melanocratic band that separates MBS from the Layered Series on Ivnarmiut (Figure 6b) has a microstructure unlike any previously described from Skaergaard. It comprises isolated, euhedral to subhedral grains of (commonly twinned) pyroxene, plagioclase, and olivine (with the modal proportions decreasing in that order), separated by a fine-grained matrix rich in oxides and containing small grains of olivine and pyroxene (Figure 9a, b). The elongate grains form a weak foliation (Figure 9a). Many of the plagioclase grains show evidence of lattice distortion (Figure 9c, d), while other large regions of plagioclase visible in Figure 9a are polycrystalline, with microstructures similar to those shown in Figure 8a. Critically, adjacent large plagioclase grains are separated by fine-grained polycrystalline plagioclase with a granular microstructure and no preferred crystallographic orientation (Figures 9c, d, e, f). Locally, this polycrystalline zone contains abundant oxide with a similar grain size (Figures 9d, e, f).

Field, microstructural, and chemical variation through the MBS

Traverse 1 (Uttental Plateau)

Traverse 1 (Figure 1), in a similar location to traverse UT of Hoover (1989a), crosses a 60m wide region rich in picrite xenolithic blocks before entering the stratigraphically lowest exposed part of the LZa subdivision of the Layered Series. The contact between the MBS and LZa is gradational (Figure 5a). There are no colloform bands in the MBS in this part of the intrusion.

The median dihedral angle is in the range 87–89˚, apart from at the inner margin of the MBS (Figure 10. The complete dataset is in Supplementary Appendix A). Θ_{cpp} rises over ~40m to a peak of 98˚ within the basal 10 – 20m of the Layered Series before decreasing to ~87˚. This positive excursion in Θ_{cpp} is seen elsewhere at the base of the Layered Series, and has been linked to the arrival of the last major pulse of incoming magma inflating the chamber to its final size (Holness *et al.*, 2007a, b; 2015).

Traverse 2 (North Kraemer Ø)

Traverse 2 is in a similar location to traverse KN of Hoover (1989a). Augite primocrysts appear between 162m and 168m from the contact. The outermost colloform band is 134m from the contact. LZb of the Layered Series begins ~270m from the contact, with an abrupt transition from coarse-grained, relatively leucocratic MBS gabbro with steeply-dipping colloform banding, into a more melanocratic Layered Series gabbro with weakly-defined modal layering that becomes more continuous and better defined over ~10m.

The spatial variation in bulk rock composition is shown in Figure 11 (with the full dataset available in Supplementary Appendix B). The bulk rock Mg# decreases steadily across the MBS, with values typical of those seen in LZa and LZb of the standard profile (Tegner *et al.,* 2009). The concentration of P_2O_5 is generally < 0.1 wt.%, with no systematic change across the MBS. Both TiO_2 and V are significantly higher in the outermost part of the Layered Series, consistent with a higher concentration of Fe-Ti oxides here (Wager & Deer, 1939).

In the outermost 100m of the MBS, Θ_{cpp} is in the range 84–87˚, with a step-wise increase to a range of 89–91˚ at ~100m (Figure 10). At ~225m from the contact, Θ_{cpp} rises smoothly over 60m to a plateau of 100–101˚, continuing into the Layered Series.

Traverse 3 (Central Kraemer Ø)

In Traverse 3, in a similar location to traverse KH6 of Hoover (1989a), the boundary between LZa* and LZb* occurs 114 - 119m from the contact. The first colloform band occurs within LZa*, about 30m from the contact. The transition to LZb in the Layered Series occurs over a few metres ~370m from the contact.

The spatial variation of Θ_{cpp} across the MBS in this traverse is characterised by a series of three plateaux at 83–85˚, 89.5–92˚ and 99–100.5˚ (Figure 10). There is a well-defined step dividing the outer two plateaux, with the two samples on each side of the step separated by 3m. The third plateau is reached by a steady increase over 30-40m: Θ_{cpp} remains constant at ~100˚ from ~250m from the contact into the Layered Series.

Traverse 4 (South Kraemer Ø)

The MBS exposed in the south of Kraemer Ø extends to MZ*: there is no LZc* in this part of the MBS. The LZa*/b* boundary is ~201m from the contact. The first colloform band is found within LZa*, some 80m from the contact. The boundary between LZb* and MZ* in this traverse (which corresponds to traverse KT of Hoover (1989a)) occurs at 290m from the contact. The boundary between the MBS and the Layered Series is ~310m from the contact, and is marked by a surface dipping ~40˚ into the intrusion dividing MBS gabbros characterised by colloform banding from weakly modally layered MZ gabbros of the Layered Series (Figure 5b). The Layered Series here contains widely-spaced faults downthrown into the intrusion that become more widely spaced, and with decreasing offsets, over ~ 100m.

The spatial variation of Θ_{cpp} across the MBS in this traverse is characterised by step-wise variation to form a series of three plateaux at 84–87˚, 91.5–93˚ and 99–100˚ (Figure 10). The outermost step is defined by two samples separated by 6m, and the second step by two samples separated by 2m. Θ_{cpp} is constant at ~ 100˚ through the cross-bedded belt and into the Layered Series.

Traverse 5 (Ivnarmiut)

The Ivnarmiut traverse was collected from the southern end of the island (corresponding to traverse IV of Hoover (1989a)), where the subdivision of the Layered Series in contact with the MBS is UZa. The contact with the adjacent Palaeogene volcanic rocks forms a steep gully between the western edge of Ivnarmiut and a small islet. The arrival of cumulus augite, marking the division between LZa* and LZb*, occurs between 85m and 100m from the contact, just inwards of the first colloform band (~75m). The first appearance of cumulus oxides occurs at ~290m, together with the loss of cumulus olivine, thus marking the division between LZb* and MZ*: LZc* is absent (Hoover, 1989a). The innermost part of the MBS here belongs to MZ*, although the adjacent Layered Series is UZa: the transition into the Layered Series occurs 350m from the contact, marked by the previously described sharply-defined, dark weathering, melanocratic zone (Figures 6, 9) that truncates colloform layering in the coarse-grained MBS (Figure 6c) and marks the start of the cross-bedded belt (shown as the grey band in Figure 12).

The spatial variation of bulk rock composition across the MBS on Ivnarmiut is shown in Figure 12 (with the full dataset available in Supplementary Appendix B). The bulk rock Mg# decreases slowly through LZa* and LZb*, with an abrupt decrease into MZ*, with values in the outermost Layered Series similar to those typical for the upper part of UZa (Tegner *et al.,* 2009). The variation of Mg# through the equivalent subdivisions of the Layered Series, as measured in the standard traverse (Tegner *et al*., 2009) is shown for comparison, with the Layered Series data stretched so the subdivision boundaries are in the same place (omitting data for LZc, and fitting the entire MZ dataset into the width of MZ*).

In a similar manner, the bulk rock normative plagioclase An mol.% decreases steadily through LZa* and LZb*, with a much steeper variation through MZ*. Again, the equivalent data from the Layered Series is shown for comparison, stretched to fit. The normative plagioclase composition (44-41 mol.% An) in the outermost Layered Series is that expected for the upper part of UZa (Tegner *et al.,* 2009). Both TiO_2 and V are high in MZ* as expected for this oxide-rich subdivision. The bulk rock P_2O_5 is low everywhere except in the outermost Layered Series, where it reaches a maximum of 0.35 wt.% before dropping back to low levels some 50m away from the edge of the MBS. The bulk rock Cu content is low throughout the MBS, with high values in the immediately adjacent UZa of the cross-bedded belt. Cu contents jump to these high

values over a very short stratigraphic range in the upper part of MZ (Nielsen *et al.*, 2015): in addition to UZ*, the more evolved parts of MZ* must consequently also be entirely missing from the MBS here.

The compositions of the primocrysts in the melanocratic band separating the MBS from the Layered Series are consistent with those expected for the upper parts of UZa (c.f. Tegner, 1997; Namur & Humphreys, 2018). Olivine has a forsterite content of 21.5-24.4 mol.%, with MnO contents of 0.83 – 0.91 wt.%, consistent with a position close to the UZa/b boundary (Namur & Humphreys, 2018). Plagioclase cores are An_{40-44}, and the cores of augite primocrysts contain 1.16 – 1.43 wt.% Al_2O_3, and 0.43 – 0.50 wt.% MnO.

The spatial variation of Θ_{cpp} across the MBS in this traverse again is characterised by step-wise variation to form a series of three plateaux at 85–86˚, 89.5–92˚ and 94–96.5˚ (Figure 10). Both steps are defined by samples separated by 5-7m. The innermost plateau is the most extensive, running from 146m from the contact into UZa of the Layered Series.

Traverses 6 and 7 (Skaergaard Mini-Peninsula)

Traverse 6 corresponds to traverse SGP1 of Hoover (1989a). The westernmost 3 samples of this traverse were collected from a group of low-lying islets. 11 samples, forming Traverse 7, were collected 140m south of Traverse 6.

LZa* is not exposed on the Mini-Peninsula. If it is assumed the contact is at the west coast of the large islet just off the Mini-Peninsula (McBirney, 1989a; Figure 1), there is a further 190m of MBS to the west of the traverse studied here. Both McBirney (1989a) and Hoover (1989a) suggest an appreciable thickness of LZc* on the Mini-Peninsula, but the case for LZc* being represented in our detailed set of samples is not convincing. Instead, there is a clear boundary between LZb* and (olivine-free) MZ* ~122m from the westernmost sample, with an abrupt transition from a coarse gabbro to a medium-grained gabbro with abundant granular oxide grains. The innermost ~10 metres of the MBS belong to UZa*, with the inner margin defined by a steeply dipping melanocratic band, ~50cm wide, rich in oxides and pyroxene, with isolated grains of plagioclase (c.f. Figure 6). The outermost Layered Series gabbros are characterised by weakly-defined modal layering offset by closely-spaced listric faults (c.f. Figure 7a). The layering becomes better defined, the faults more widely spaced, and the displacement associated with each fault smaller (c.f. Figure 7c), over ~100m into the intrusion. Primocryst apatite first appears in the cross-bedded belt at ~230m. The relatively steep dip of the (multiply-faulted) layering in the cross-bedded belt resulted in an unavoidable move 18-23m up-stratigraphy in the Layered Series at the end of the traverse (Figure 10).

The shorter, and less detailed, Traverse 7 begins in LZb*, with LZb* separated from MZ* by a single sample representing LZc*: the lowest appearance of LZc* on the western wall of the intrusion therefore occurs somewhere between Traverses 6 and 7 (Figure 2). The innermost two samples of Traverse 7 comprise UZa*. The lack of detailed sampling prevents tight constraints being placed on the width of the subdivisions, but the two Mini-Peninsula traverses can be correlated by placing the single Traverse 7 LZc* sample at the LZb*/MZ* boundary of Traverse 6: the coincidence of the dihedral angle measurements (Figure 10) supports this correlation.

The variation of Θ_{cpp} through Traverse 6 is complex, with two well-defined step-wise changes (both defined by pairs of samples separated by 5m) forming an outermost plateau at 89-91˚, a subsequent plateau at 95-97˚, and then a zone beginning 134m from the contact where Θ_{cpp} is in the range 100-103˚ over ~40m

before a steady and sustained decrease to a minimum of 88˚ in the base of UZb in the Layered Series (~266m from the start of the traverse). Θ_{cpp} then increases to 94.5˚ over the remaining 65m of the traverse along strike in UZb.

Traverse 8 (Skaergaard Peninsula)

The contact with the country rocks is not exposed but is close to the present coastline. In Traverse 8, corresponding to traverse SPN of Hoover (1989a), cumulus augite appears 60-69m from the western end, with cumulus oxides appearing at ~400m. The evidence for LZc* being present in the MBS here, as suggested by Hoover (1989a), is not compelling, as olivine is present in very small quantities from 400m, and entirely absent from ~430m: we have correspondingly assigned all these rocks to MZ*. The outermost colloform band occurs within LZb*, 105m from the contact.

Though olivine is present in some samples further than ~500m from the western end of the traverse, it only becomes abundant in samples more than ~564m from the western end, marked in the field by a change to a heavily weathered and crumbly character. The first sample encountered with high bulk rock Cu concentration (corresponding to upper MZ) is sample SP27, 564m from the western end of the traverse (Nielsen *et al*., 2015). Although Nielsen *et al.* (2015) assign this sample to MZ* on the basis of its low Pd/Pt ratio, the composition of plagioclase determined from the CIPW norm is An_{46} (Figure 13; Supplementary Appendix B), consistent with it belonging to UZa*. On the basis of the normative plagioclase composition, we therefore assign SP27 to UZa* and place the MZ*/UZa* boundary between 558m and 564m from the contact (with the outermost Cu-rich bulk compositions therefore falling somewhere in the 25m separating samples SP27 and SP25). Abundant apatite primocrysts appear at 586m, which must therefore mark the beginning of UZb*. These observations point to UZa* on the Skaergaard Peninsula being 22 - 28m wide, similar to the thickness of UZa* on the Mini-Peninsula, contradicting the suggestion of Hoover (1989a) that UZa* is significantly wider than MZ* here. The Layered Series, comprising UZb, begins at about 650m from the start of the traverse, with the cross-bedded belt extending to 695m.

The bulk rock chemistry of a sub-set of samples from this traverse has been presented by Nielsen *et al.* (2015): a fuller dataset is shown in Figure 13. The Mg# and normative plagioclase composition are compared to that in the standard profile of Tegner *et al*. (2009).

The Mg# in much of the MBS varies smoothly and falls within the scatter of the equivalent subdivisions in the Layered Series (Figure 13). Mg# in the two samples from UZa* is lower than that observed for almost all UZa samples in the Tegner *et al*. (2009) standard profile, while there is comparably less variation in UZb* than in the (albeit complete) UZb. The normative plagioclase composition in the MBS maps closely onto the values in the standard profile. In the latter, the boundary between UZa and UZb corresponds to a normative plagioclase composition of ~42 mol.% An. The normative plagioclase compositions in our two UZa* samples fall in, or close to, the range seen in the Layered Series UZa. In contrast, the normative plagioclase compositions in both UZb* and the extension into the Layered Series on the Skaergaard Peninsula are almost all lower (~30 mol.% An) than in the equivalent UZb (42 – 33 mol.% An), perhaps reflecting the high fraction of evolved liquids in the inner parts of the MBS and the outer parts of the Layered series on the Peninsula. The bulk rock P_2O_5 concentration peaks in UZb*, as expected, with a rapid decrease towards the Layered Series, indicative of an initial overproduction of apatite immediately following its arrival as a liquidus phase. TiO_2 is relatively high throughout MZ* and UZa*, decreasing through UZb*

into the Layered Series. V increases from LZa* to LZb*, presumably because of the increased mode of interstitial Fe-Ti oxides (as indicated by the increase in TiO_2, Figure 13) as the interstitial liquid becomes more evolved.

The variation of Θ_{cpp} through the MBS on the Skaergaard Peninsula comprises four clearly distinguishable plateaux (Figure 10), separated by step-wise increases which are defined by pairs of samples separated by 5m, 10m and 2m (from the margin inwards). The outermost plateau is at 81.5-84˚, followed successively by those at 85-87˚, 90-92˚, and 98-100˚. This innermost plateau is over 100m wide and is followed by a smooth decrease of Θ_{cpp} to a minimum of 90˚ in the cross-bedded belt, followed by a steady increase to ~100˚ over some 70m along strike in the Layered Series. Note, however, that there is a gap in the data spanning almost 100m at the outermost region of the Layered Series, due to the scarcity of suitable grain junctions in these coarse-grained samples.

Traverse 9 (Vandfaldsdalen)

The Vandfaldsdalen traverse, on the eastern margin, comprises widely-spaced samples and is incomplete: the inner contact with the Layered Series is not exposed. The outermost regions of the MBS contain cumulus olivine and plagioclase: augite joins this assemblage between 154m and 162m from the contact. Θ_{cpp} forms two plateaux, one at 86 – 87˚, and the other at 93 – 95˚ (Figure 10).

Layered Series - UZb

In the most evolved parts of the intrusion, where macro-dolerites are present, the interpretation of Θ_{cpp} requires an assessment of the amount of retained late-stage liquid (Holness *et al*., 2017a). The volumetric proportion of late-stage paired granophyric and ilmenite-rich intergrowths (representing the Si-rich and Fe-rich conjugates, respectively, of an unmixed immiscible interstitial liquid: Holness *et al*., 2011) is shown as a function of distance along strike through UZb, from the MBS to the top of drill core 90-10 on the Skaergaard Peninsula, in Figure 14.

The volumetric proportion of both types of intergrowth follow similar trends, with low abundance (< 15 vol.% in total) in the inner parts of the MBS, climbing steeply over a few tens of metres to a maximum of 30 vol.% (total) at the outer edge of the cross-bedded belt. The volumetric proportions then fall steeply through the cross-bedded belt, with a more gradual rate of decline in the marginal regions of the Layered Series. The proportion of granophyre is everywhere higher than that of the ilmenite-rich intergrowths, denoting a dominance of the Si-rich conjugate of the immiscible liquid, with the relative enrichment decreasing from a maximum in the cross-bedded belt to near-parity towards the top of drill-core 90-10 (Figure 14). At the collar of drill core 90-10, the total volumetric proportion of these late-stage intergrowths is ~10%. This is similar to the value of 10 wt.% trapped liquid in drill core 90-10 calculated from P_2O_5 in UZa reported by Holness *et al*. (2017a), but somewhat higher than the values of 3 – 11% calculated by Tegner *et al.* (2009) for the reference profile, averaging just below 5 wt.% through UZa where sampled by drill core 90-22 (Figure 1).

DISCUSSION

Differences in grain size between the MBS and the Layered Series

Perhaps the most conspicuous characteristic of the MBS is its generally much coarser grain size compared to the equivalent gabbros of the Layered Series. Dolerite dykes tend to be coarser-grained than sills of the same thickness (Philpotts & Ague, 2009, p. 85), attributable to the growth of plagioclase as isolated grains suspended in convecting magma in dykes, in contrast to sills in which absent or weak convection means that crystals nucleate and grow *in situ* on the roof and floor (Holness *et al*., 2017b). We might therefore expect the MBS to be finer-grained than the Layered Series, since the former grew predominantly by *in situ* nucleation, whereas the latter is dominated by an accumulation of grains grown elsewhere in the chamber (Irvine *et al*., 1998; Holness *et al*., 2020). The apparent discrepancy can be explained if the floor cumulates were formed of abundant relatively small grains for which any post-accumulation growth is stopped by early impingement with their closely-spaced neighbours, whereas the large grain size of the MBS results from comparatively greater spacing between grains nucleated *in situ* that can then grow significantly before impingement.

The thermal structure of deep, km-scale, magma bodies which are closed to magma input (Irvine, 1970) precludes significant nucleation of crystals *on* the chamber floor itself, due to the low thermal gradient through the thick floor accumulation and the latent heat hump of Morse (1986; 1988). Most nucleation is thought to occur at the roof and walls, or in downwelling convection currents *near* the floor (Irvine, 1970; Morse, 1986; 1988). The high thermal gradient and relatively thin mush at the walls, together with the likelihood of continuous downwards convective flow of the adjacent bulk magma (driven by both cooling and by fractionation), might lead one to expect a high rate of heterogeneous nucleation at the inner margin of the wall mush, in contrast to the low concentration of nucleation sites indicated by the coarse grain size of the MBS: this apparent discrepancy might be a result of poor retention of crystals nucleated at the wall.

Addition to MBS of material crystallised elsewhere

The clusters of euhedral olivine grains observed in the MBS are highly unlikely to have formed by impingement of olivine grains nucleated *in situ* at the walls, as this results in irregular grain boundaries with no orientation relationship to the crystallographic orientation of the adjacent grains (Holness *et al*., 2019), rather than the planar grain boundaries parallel to low index faces which are observed (Figure 8c). Instead, these clusters most probably formed by synneusis of grains that had attained their final size as isolated grains (e.g. Wieser *et al.,* 2019). We suggest that grain clusters formed in the convecting bulk magma were captured by the rough, inner margin of the wall mush in an analogous manner to the trapping of clusters of olivine grains at the roof of the convecting Shiant Isles Main Sill (Holness *et al.,* 2017d): at least some of the material in the wall mush was therefore grown elsewhere. This, together with the abundant evidence of both continuous and episodic collapse of the wall mush (see later discussion) suggests a complex interaction between the different regions of the intrusion.

The appearance of abundant grains of twinned augite at the LZa*/b* (and LZa/b) boundary, and their presence throughout the remainder of the MBS and Layered Series, is most probably a consequence of the greater difficulty in nucleating a crystal either homogeneously in bulk magma, or heterogeneously on the inner margin of the wall mush, compared to within the pores of a crystal mush. While the energetic barrier to creating a twinned embryo is higher than that for an untwinned embryo (Kato & Cahoon, 1985), its growth rate is faster (Becke, 1911), making it more likely that twinned embryos grow into stable nuclei.

Their elongate shape, compared to untwinned primocrysts in the same sample, is an example of the well-known phenomenon of twinned grains growing with a different habit to untwinned grains (Lee *et al.,* 2003): the elongation parallel to the twin plane is most likely a consequence of either a high density of screw dislocations within the twin plane (Kitamura *et al*., 1979), or the ease with which atoms are added at the surface at the re-entrant formed by the intersection of the (100) twin plane with the (001) face (Lee *et al*., 2003).

The comparative rarity of twinned interstitial augite in both LZa and LZa* suggests that there is no advantage associated with lattice defects in augite grains nucleating heterogeneously within the pore space. The presence of twinned augite primocrysts in both the MBS (Figure 8e) and in the Layered Series, the euhedral morphology of those in the MBS, and the observation that twinned grains are dominant in the localised augite-rich parts of the MBS, suggests that, in an analogous manner to the MBS olivine clusters, at least some of the MBS twinned augite grains may have nucleated and grown elsewhere, perhaps in the bulk magma or at the roof, before being captured by the inner margin of the MBS.

The generally euhedral nature of the Fe-Ti oxide grains in MZ* and MZ in the outermost Layered Series contrasts with their more irregular morphology in the central part of the chamber floor, where euhedral grains are almost invariably inclusions in grains of other minerals. An irregular morphology is due to post-accumulation overgrowth from interstitial melt containing abundant ponded immiscible Fe-rich liquid (c.f. Holness *et al*., 2011; Nielsen *et al*., 2015). The vertical geometry of the MBS means that any buoyancy-driven flow of interstitial immiscible conjugates is parallel to the wall. This means that it is not possible to generate concentrations of the immiscible Fe-rich conjugate in the MBS, as is argued to have occurred in the floor cumulates, because any dense liquid flowing downwards from overlying regions is compositionally similar to that which has already been lost, consistent with the absence of reactive symplectites in the MBS (Holness *et al*., 2011). The outermost Layered Series also contains euhedral Fe-Ti oxide primocrysts, again suggesting a lack of late-stage growth from immiscible Fe-rich liquid. This may be a consequence of a thicker than usual mush (e.g. Holness *et al*., 2017a), in which the immiscible conjugate interstitial liquids act much as those in the MBS, with little segregation due to differential flow.

What caused changes in Θ_{cpp} in the MBS?

There are sharply-defined step-wise increases in Θ_{cpp}, occurring over a few metres, in all traverses across the MBS (Figure 10), similar to that in other continuous sequences of progressively fractionated rocks (Holness *et al*., 2013). In addition to the step-wise changes, in several of the traverses Θ_{cpp} exhibits steady increases or decreases over distances of some tens of metres in the innermost parts of the MBS (Figure 11). Two of the structurally lowest traverses (North and Central Kraemer Ø), are remarkable for extended ramped increases in Θ_{cpp}, bringing the values in the innermost parts of the MBS up to those of the adjacent Layered Series, while those on the Mini-Peninsula and the Skaergaard Peninsula decrease progressively to the outermost Layered Series before increasing again.

We suggest, following Holness *et al.* (2013), that the sharply-defined step-wise changes are caused by the addition of a new liquidus phase to the magma adjacent to the wall mush, changing the contribution of latent heat to the enthalpy budget and thus plagioclase grain shape. Thus, the steps correspond to the

progressive addition of augite, Fe-Ti oxides and apatite to the liquidus assemblage, with all three steps present only on the Skaergaard Peninsula, where the MBS is most complete. The values of Θ_{cpp} in the MBS corresponding to each liquidus assemblage change with increasing height up the intrusion wall (i.e. from north to south) and differ from their Layered Series equivalents (Table 1), potentially providing information about cooling rates in different parts of the intrusion. In a similar manner to the Layered Series, the step-wise increases in Θ_{cpp} are generally off-set from the appearance of the additional liquidus phase and, in some cases, occur without the relevant subdivision being present in the MBS. This not only demonstrates significant loss of material from the wall mush (with the immediate follow-up question of where this material ended up), but also provides constraints on its thickness (e.g. Holness *et al.*, 2017a, c). Finally, the variation of Θ_{cpp} at the innermost edge of the MBS, through the cross-bedded belt, and into the adjacent Layered Series demonstrates the spatial (and temporal) extent of the effects of the enthalpy budget of the encroaching floor mush. Each of these points is addressed in the following sections.

Evidence of loss of wall mush

Although Hoover (1989a) argued that the reason for the first appearance of each subdivision occurring at a structurally higher level than the corresponding subdivision in the Layered Series (Figure 2) is that there were differences in magma composition at the walls and floor, we argue that it is, instead, a consequence of the loss of material from the developing wall mush. In this section, we place constraints on this loss, using the variation of Θ_{cpp}, the rate of compositional change in comparison to that observed in the Layered Series (e.g. Tegner *et al.*, 2009; Namur & Humphreys, 2018), and the thickness of each subdivision in the MBS compared to its Layered Series equivalent (e.g. Nielsen, 2004; Tegner *et al.*, 2009).

Perhaps the clearest evidence for significant loss of material is the absence of LZc* from much of the wall above the level of the LZb/c boundary in the Layered Series (Hoover, 1989a), even though the spatial variation of Θ_{cpp} shows that LZc* material was certainly present, if only transiently, on the inner margin of the MBS. Traverses 4 and 5 (South Kraemer Ø, Ivnarmiut) each contain a pair of step-changes of Θ_{cpp} (Figure 10). The outermost of each pair occurs at, or just offset outwards from, the LZa*/LZb* boundary and, by association must be related to the arrival of cumulus augite. The inner step-change must therefore be associated with the arrival of cumulus Fe-Ti oxides, but there is no corresponding LZc* (Figure 2). A similar situation is found further south: the outermost of the two step-changes in Traverse 6, and the second of the three steps in Traverse 8 (Figure 10), must be associated with the arrival of cumulus oxides, despite the absence of convincing LZc* material. Since these step-changes in Θ_{cpp} are caused by the increased contribution of latent heat to the enthalpy budget following the addition of Fe-Ti oxides to the primocryst assemblage, the LZc/LZc* liquidus assemblage must have been crystallising on the inner MBS margin wall here and, by extension, over the entire western wall after the saturation of the bulk magma in oxides. The step-wise increase in Θ_{cpp} is the smoking gun pointing to the fact that gabbroic mush with the LZc* assemblage has been lost from the MBS.

Such loss of material from the MBS was not confined to LZc times. Comparisons of the widths of the various MBS subdivisions in Traverse 8 (Skaergaard Peninsula) with those in the standard profile through the Layered Series (Tegner *et al.*, 2009) shows that the thickness of LZb* is proportionately almost twice

the thickness of LZb in the Layered Series, MZ* is half as thick as MZ, and UZa* is only 1/7 the expected thickness from comparison with UZa (with UZa* entirely absent from Ivnarmiut just to the north, even though the immediately adjacent Layered Series belongs to UZa). These differences are clearly shown by the changes in spacing of the compositional data from Tegner *et al*. (2009) across the MBS on the Skaergaard Peninsula (Figure 13): the Tegner *et al*. sample spacing was approximately constant through the Layered Series, but the fitting of their data onto the MBS traverses requires stretching by varying amounts in the different subdivisions. The rate of change of plagioclase composition through much of the Layered Series stratigraphy is constant (Tegner *et al*., 2009; Namur & Humphreys, 2018) but the MBS plagioclase compositional evolution on the Skaergaard Peninsula shows a steepening in slope at the start of MZ*, and a marked break in slope at the start of UZa* (Figure 13). Similar features are present in the less complete Traverse 5 on Ivnarmiut (Figure 12). The relative over-representation of LZb* on the Skaergaard Peninsula compared to the under-representation of MZ* and UZa* is either a consequence of different rates of accretion of material to the wall mush through time or to different rates of loss.

Further evidence of loss of material is provided by the compositions of the primocrysts in the melanocratic band separating the MBS from the Layered Series on Ivnarmiut (Figure 6), which are typical of those in the upper parts of UZa. Although we cannot determine whether individual grains were derived from the MBS or the adjacent Layered Series on the basis of composition alone, it is suggestive that UZa material was present on the walls and has been subsequently entirely lost, leaving MZ* in contact with upper UZa at this point on the wall.

What caused the loss of material from the wall?

There are several different ways in which material might have been lost from the walls: a series of major catastrophic collapse events, a series of smaller collapses more closely spaced in time, or simply by poor retention of material at the inner margin of the mush leading to a continuous loss. The new evidence for decreased mush retention or accretion from LZc* to UZa* is consistent with the published evidence for an increasingly poorly consolidated mushy zone on the inner margin of the MBS as it got thicker (Humphreys & Holness, 2010; Namur *et al.,* 2013; see later), suggesting an increasingly important contribution from continuous loss of poorly retained material with time. The marked increase in the density of the primocryst assemblage from LZc* onwards (*c.f.* Tegner *et al*., 2009) may have also contributed to an increased rate of continuous loss. This increase in density is compounded by the commonly equant shape of primocryst oxide grains (*e.g*. Wager & Brown, 1968), which would generate a less mechanically coherent mush framework at a given melt porosity than one formed of (randomly oriented) elongate grains. However, the good representation in the MBS of the relatively oxide-rich subdivisions from MZ* onwards suggests that a further mechanism is needed to explain the almost complete absence of LZc*. We suggest that loss of LZc* was amplified by significant tectonic disruption in late LZc times.

The Skaergaard intrusion formed in a tectonically active, extensional setting: the stratigraphically localised distribution of roof blocks on the floor (Irvine *et al*., 1998) is consistent with episodic shaking of the intrusion by contemporaneous fault movement. We suggest that the anomalous asymmetry of MZ, which is thicker by several hundred metres in the west compared to the east (McBirney, 1989a; Nielsen, 2004), is a consequence of tilting of the entire intrusion towards the west or southwest during active extensional

faulting of the Greenlandic margin in late LZc times. The associated earthquakes could have dislodged poorly consolidated material from the walls. If the entire LZc* were poorly consolidated, this could account for the almost complete absence of LZc* in the MBS. A period of relative quiescence through MZ would result in the re-establishment of a symmetrical shape of the magma-mush interface on the chamber floor.

The truncation of the colloform banding in the outermost MBS on Ivnarmiut (Figure 6), which is seen nowhere else on the western margin, suggests that the absence of UZa* here was also due to a catastrophic collapse event. This is supported by the microstructures observed in the melanocratic band at the edge of the MBS in this region of the wall. Firstly, the dominance of isolated euhedral grains, and absence of evidence of a framework (Figure 9a), suggests the breakup of a mush zone. That this breakup was accompanied by shearing of the crystal-rich material is shown by the evidence for plastic deformation of the large plagioclase grains (Figure 9c, d). Perhaps most significantly, the fine-grained bands separating the large plagioclase grains are similar to those reported from the Bushveld intrusion by Vukmanovic *et al*. (2019) and ascribed to cavitation-driven nucleation within a sheared crystal-rich mush. Similar neoblastic zones in gabbros of the Basement Sill, Antarctica, were suggested to have formed by recrystallisation triggered by deformation by Bedard *et al*. (2007). The melanocratic band on Ivnarmiut and the Mini-Peninsula may represent the surface separating material that was sufficiently well-consolidated to resist collapse from that which was lost to the floor. The presence of olivine primocrysts in the melanocratic band, and mineral compositions which are typical of those for UZa, suggest that at least some UZa* material was incorporated during shearing. The localised occurrence of the melanocratic band and the associated truncation of colloform banding demonstrates that the loss event that it records was highly unusual, penetrating deep into the MBS. The UZb subdivision of the Layered Series shows the same asymmetry as does MZ, being thicker in the west (Nielsen, 2004). We suggest that this asymmetry was also caused by an episode of faulting associated with extension of the Greenlandic margin, and that the earthquakes associated with this faulting were sufficiently strong to disrupt the inner parts of the MBS.

Where did the lost wall material end up?

The evidence, documented above, for loss of significant amounts of material from the MBS begs the question of where this material ended up: the most likely place is the chamber floor (e.g. Upton, 2013). The cross-bedded belt probably hosts at least some of the lost material, although the abundance of erosion horizons and unconformities (Figure 5a) suggests that this region cannot be the final resting place of much of it, which must have been carried further across the intrusion floor by convection currents pouring off the walls (Wager & Deer, 1939; Wager & Brown, 1968; Irvine, 1980). The more melanocratic nature of the marginal parts of the Layered Series compared to the same layers nearer the centre of the floor (Wager & Deer, 1939), may be a record of this winnowing process, with the dense minerals accumulating near the walls while the more buoyant plagioclase was able to move further across the floor.

We suggest that whereas crystals and crystal clusters lost during continuous attrition of poorly consolidated material are likely to have been disseminated widely across the floor by convecting magma, with a consequent difficulty of identifying their origin in the MBS, episodes of catastrophic loss of large amounts of material are more likely to be visible in the Layered Series. The upper parts of LZc are notable for a series of highly oxide-rich, 0.5 - 2m thick, layers within a ~30m section of stratigraphy across most of the

intrusion floor (Bollingberg, 1995; Weatherley *et al*., 2018). The oxide-rich horizons are commonly associated with cognate xenoliths, likely sourced from the roof, up to 400 m long. These layers, clearly associated with a destabilisation of the UBS (and therefore likely to be associated with tectonic activity) are plausible candidates for the final resting place of material lost from the inner part of MBS during LZc times (Weatherley *et al*., 2018).

The collapse of the inner regions of the wall mush during UZa times most likely contributed to the localised thick mushy layer (analogous to a talus slope) on the outer parts of the floor recorded at the UZa/b boundary where sampled by the 90-10 drill core (Figure 10; Holness *et al*., 2017a). Notably, Wager & Deer (1939) report abundant, unusually large, grains of olivine and (highly elongate) plagioclase in one of their melanocratic samples from the margins of UZa on Ivnarmiut: such large grains are plausible candidates for material sourced from the MBS. We will explore the spatial distribution of the large elongate plagioclase grains, and the implications of the sudden change in surface topography near the wall for the convective regime, and localisation of crystal-laden currents, in a future contribution.

The thickness of the crystal mush

The thickness of the mushy zone can be constrained at those points where a new phase is added to the liquidus assemblage (Figure 7b). Note that the loss of the inner, high-porosity, parts of the growing wall mush means that this method underestimates mush thickness, particularly when thickness is estimated using the Θ_{cpp} step associated with oxide-in which, due to the absence of LZc*, we must pair with the position of the LZb*/MZ* boundary.

The mush thickness during the early stages of solidification can be constrained by the off-set between the first appearance of equant twinned augite and the associated step-change in Θ_{cpp} (Figure 10). The mush at augite-in was only a few metres thick on South Kraemer Ø, and 0-11m thick on the Skaergaard Peninsula. It was thicker elsewhere, with 11-31m on Ivnarmiut, 18-47m in Vandfaldsdalen, 28-51m on North Kraemer Ø and 0-19m on Central Kraemer Ø.

The dihedral angle step associated with the arrival of cumulus oxides is offset by 83-106m from the LZb*/MZ* boundary on the Skaergaard Peninsula, and at least 65-77m on the Mini-Peninsula. The minimum thickness of the wall mush recorded by the step-wise increase associated with the LZb*/MZ* boundary in Traverses 5 (Ivnarmiut) and 6 (South Kraemer Ø) are 127-150m and 24-31m respectively.

The final point at which mush thickness can be constrained is at the moment the bulk magma became saturated in apatite. The step-change in Θ_{cpp} is observed on the Skaergaard Peninsula where it is offset by 169-187m from the first appearance of primocrystic apatite (Figure 10). On the Mini-Peninsula, the step-change in Θ_{cpp} associated with apatite-in must have formed after the MBS had been covered by the rising floor mush, since the arrival of apatite as a liquidus phase post-dates the cessation of growth of the MBS. Placing the edge of the MBS at the beginning of the cross-bedded belt, the outermost 76-91m of the MBS was mush at the moment the rising floor cumulates encroached.

Mush thickness does not vary in any consistent manner with position on the magma chamber wall. However, there is a general increase in mush thickness as the overall MBS becomes thicker (Figure 15).

This is consistent with a decreased heat flux through the wall as the insulating effects of the MBS increase, and in agreement with inferences about increasing mush thickness from the morphological evolution of both late-stage tears in the mush (Humphreys & Holness, 2010) and the colloform bands (Namur *et al*., 2013). There are two places where there are outliers from this general trend. Firstly, the mush on the south of Kraemer Ø is thinner than expected: LZb* here is also much thinner than elsewhere (e.g. half the thickness seen at the centre of Kraemer Ø and on Ivnarmiut, and a third of the thickness seen on the Skaergaard Peninsula). Given the absence of any general correlation with country rock lithology (i.e. gneiss vs plateau basalt), and therefore rate of heat loss, a thin mush zone is likely a consequence of loss of poorly consolidated material at the inner margin. From comparison with the thickness variations in other traverses (Figure 15), we might expect the MBS in the south of Kraemer Ø to have lost ~30m of loosely-consolidated material. That it is thin at both the augite-in and the oxide-in steps tells us that this loss was likely to have occurred from late LZa* onwards, continuing during the formation of LZb*.

In contrast, the mush on Ivnarmiut during LZb times was thicker than expected, with at least half of the total 300m thickness of the wall material being incompletely solidified. It is tempting to speculate that the continuous loss of material during MZ times suggested by the compositional data, and the major loss of material during UZa times, from this part of the wall was a consequence of the mushy zone here being exceptionally thick: by UZa times it had become unsustainable. An earthquake in UZa times, associated with crustal extension, would then have triggered the catastrophic collapse argued for earlier.

Why do we see exceptionally thick mush on Ivnarmiut, but thinner-than-expected mush on the south of Kraemer Ø? The thickness of the mush at any time depends on the rate of heat removal, and the details of its structure which control the critical point of failure under gravity. Given that the thermal gradient through the intrusion sidewalls was horizontal, we can assume that the grain-scale structure of the mush in a given subdivision would have been very similar at the two heights represented by these two profiles through the MBS. Given the absence of changes in grain size, or any relationship between mush thickness and country rock lithology, we speculate that the geometry of the wall must exert a primary control on mush thickness, with thicker mush found above ledges. A ledge at the unconformity between Palaeogene volcanics and gneiss (Figure 2) would support and stabilise a greater thickness of mush on the upper part of the wall (Ivnarmiut), preventing or reducing attrition from the inner margin, while reducing the strength of the mush below the ledge (Southern Kraemer Ø) which would not be supported by cohesion with overlying material. Seismic activity could then dislodge the mush above the step, triggering the catastrophic collapse of the MBS both at Ivnarmiut and higher parts of the wall, which would no longer be supported once Ivnarmiut had given way. Interestingly, although Hoover (1989a) and Irvine *et al*. (1998) suggested the faulted off-set of the contact on Kraemer Ø (Figure 1) enabled the accumulation of xenoliths during the earliest history of the Skaergaard, faulting is unlikely to have resulted in a significant shallow-dipping ledge as there is no compelling evidence that the off-setting fault was low-angle (c.f. Nielsen, 2004).

Where the first colloform band occurs within the outer parts of LZa*, before the outermost step in Θ_{cpp} (in Central and South Kraemer Ø), it is not possible to place any constraints on the thickness of the mush in which they form. However, on North Kraemer Ø, Ivnarmiut and the Skaergaard Peninsula, the first colloform occurs 105-134m from the contact - further than the outermost step in Θ_{cpp} - suggesting that colloform bands form 20-50m from the inner margin of the mush (Figure 15). The truncation of colloforms

at the edge of the MBS on Ivnarmiut (Figure 7c) therefore suggests that at least 20-50m of mush must have been lost during the UZa collapse event.

Spatial variations of Θ_{cpp} in the intrusion: MBS vs Layered Series

There is no clear difference between Θ_{cpp} in the traverses in Vandfaldsdalen and Central Kraemer Ø, the most likely stratigraphic equivalents. This is consistent with Hoover's (1989b) suggestion that the eastern and western walls of the intrusion cooled at the same rate: the greater hydrothermal circulation in the highly fractured basalts forming the intrusion's eastern wall compared to the lower permeability gneisses of the western wall (Taylor & Forester, 1979) did not affect the MBS during LZ times.

If we assign each of the plateau regions of Θ_{cpp} to mineralogical zones, ignoring the offset between the step-change and the actual zone boundary, Θ_{cpp} gradually decreases upwards (Table 1), with the lowest values of Θ_{cpp} for all zones in the MBS, found in Traverse 8 (Skaergaard Peninsula). This is consistent with the expected greatest heat loss at the top corners of a box-like intrusion (*e.g.* Nielsen, 2004)

Values of Θ_{cpp} associated with the LZa* primocryst assemblage (Table 1) are similar to those of LZa (Figure 7), while those associated with the LZb* assemblage (Table 1) are invariably significantly lower (85 – 93˚) than LZb (95-100˚; Table 1). Values associated with the primocryst assemblages of subdivisions LZc*, MZ* and UZa* are similar to those of the equivalent Layered Series subdivisions in the lower parts of the wall, but fall significantly below in the upper parts of the wall. Those few MBS samples recording the thermal effects of the addition of apatite to the liquidus assemblage reach a maximum of ~100˚, compared to ~105˚ in the Layered Series equivalents. These generally lower values are consistent with the expected more rapid cooling rate of the wall mush, particularly those parts of the wall mush close to the roof, compared to the floor.

Detailed comparison of Θ_{cpp} in the most evolved parts of the MBS (i.e. Traverses 5-8) and their Layered Series equivalents is not straightforward because Layered Series rocks from UZa and UZb have highly variable Θ_{cpp} depending on the amount of interstitial liquid (Figure 7; Holness *et al*., 2017a). The closest Layered Series equivalent examined by Holness *et al*. (2017a) is core 90-10 (Figure 1): UZ in this core contains abundant interstitial liquid (Figure 14), with the first appearance of macro-dolerite in UZb (Figure 7b). The Ivnarmiut profile ends in UZa and, similar to 90-10, shows no evidence of macro-dolerite in UZa. Both the Skaergaard Peninsula and the Mini-Peninsula traverses end in UZb, displaying the step-change to high Θ_{cpp} associated with apatite-in. As in core 90-10 (Holness *et al*., 2017a), these high values are transient, retained only the mid-point of MZ* before a sustained decrease through the remaining MBS.

The transition from MBS to the Layered Series

The inner margin of 5 traverses is marked by an extended transition to Θ_{cpp} values typical of the adjacent Layered Series (Figure 10, Table 1). In the structurally lower parts of the wall this is manifest as an increase in angles, and in the upper parts by a decrease. We can account for the extended increase of Θ_{cpp} in the

lower parts of the wall (North and Central Kraemer Ø) by considering the evolving positions of the chamber floor. In the early stages of wall solidification, the chamber floor was distant, and Θ_{cpp} in the outer MBS was controlled by the local enthalpy budget. Crystal accumulation brought the floor closer, with the inner margin of the MBS denoting the point at which its inwards growth was arrested by the encroachment of the Layered Series. The increasing Θ_{cpp} within the inner parts of the MBS denotes a slowing of the cooling rate due to the influence of the enthalpy budget (essentially, the latent heat hump of Morse (1986)) of the approaching floor.

In the north of Kraemer Ø, the thermal effects of the chamber floor begin some 50m from the edge of the MBS, so this point marks the outer edge of the mushy inner part of the MBS at the moment the floor was sufficiently close to influence the cooling history of the wall mush. The mush was ~50m thick at the point the floor encroached (Figure 15), so the ramp we see begins only once the floor had arrived at this level on the wall. In the centre of Kraemer Ø, the ramp begins ~235m from the contact. The MBS here is 355m wide, suggesting 90 - 110m thickness of mush (Figure 15), again consistent with the thermal influence of the encroaching floor being felt only when the floor was close to this level on the wall.

In the structurally highest parts of the intrusion, Θ_{cpp} decreases in the inner parts of the MBS as the cross-bedded belt is approached, followed by an increase further east along strike into the Layered Series. This variation is well defined for the Mini-Peninsula traverse (Figure 10), and the few well-constrained data points on the inner parts of Traverse 8 on the Skaergaard Peninsula show the same trend (the data from the small populations obtained from intervening samples in Traverse 8 support this: Supplementary Appendix A). An increase in Θ_{cpp} is also observed in the topmost few metres of drill core 90-10 (Figure 7b). The reason behind these changes in Θ_{cpp} is not clear. The increase seen in the two traverses cannot be a consistent stratigraphic effect, since it is observed along strike at different stratigraphic levels. It must instead be a consequence of the proximity of the contact with the country rock. Although it is possible that there is some effect of a higher cooling rate in this top corner of the intrusion, we suggest the low angles in the vicinity of the cross-bedded belt might be controlled by the composition of the retained interstitial liquid. An abundance of granophyre in the cross-bedded belt at this part of the wall (Figure 14) would lead to a more macro-doleritic character (c.f. Holness *et al.*, 2017a) that reduces in significance both inwards and outwards towards the wall as the volumetric dominance of granophyre (relative to the ilmenite-rich intergrowths) decreases.

CONCLUSIONS

Although the Skaergaard floor cumulates are generally thought to be accumulations of material predominantly nucleated and grown mostly at the roof (Irvine, 1970; Morse, 1986; 1988), we argue that at least some component of the Layered Series was derived from the highly unstable mush developing on the vertical intrusion walls. The MBS lost material, likely both by a continuous rain and by episodic collapse triggered by earthquakes in the extending Greenlandic margin. The rate of continuous loss from the walls (and rate of accumulation at the floor) was significantly increased once Fe-Ti oxides became part of the liquidus assemblage, perhaps due to a significant decrease in the cohesion of the mush associated with a

higher proportion of equant dense grains. That the region of the wall now exposed on Ivnarmiut was especially susceptible to failure may have been because of the unusually thick poorly consolidated mush, perhaps a consequence of irregular wall geometry. Despite ongoing loss of poorly consolidated material, the thickness of the mushy zone increased as the MBS itself grew thicker, to a maximum of ~180m in the later stages of solidification of the entire intrusion.

Although the Skaergaard intrusion is perhaps unusual in its large expanse of essentially vertical walls, our detailed examination of the mush on those walls has a more general applicability to other crustal magma bodies, particularly vertically extensive conduits such as macrodykes (e.g. White *et al.*, 1989; Upton, 2013). Crystallisation on steeply-dipping surfaces is clearly a highly dynamic process, with loss of material driving fractionation and creating cumulates in nearby, gravitationally stable, locations. The abundance in the Skaergaard wall mush of crystal clusters formed by synneusis demonstrates that mass transport was not entirely in one direction in the intrusion, with crystals grown at the roof or in the bulk magma being added to the MBS, as well as the MBS supplying material to the floor: this complex interchange of material from the various solidification fronts is probably only possible in convecting systems. That the wall mush could attain thicknesses of several hundred metres provides constraints on the length-scales of vertical mushes in settings such as sub-volcanic feeder conduits.

ACKNOWLEDGEMENTS

MBH is indebted to Galahad Gold plc, and in particular Morris Beattie, for the generous provision of logistical support during the 2006 field season. Platina Resources were accommodating and helpful during the 2008 and 2011 field seasons. The 2017 field season relied on logistical support from GEUS. Fieldwork was funded by the Royal Society, the Carlsberg Foundation, GEUS, the Natural Environment Research Council [grant numbers NE/N009894/1 and NE/J020877/2], Trinity College, and the University of Cambridge. Help in the field was provided by Gemma Stripp, Brendan Dyck, Sam Weatherley, Gautier Nicoli and Victoria Honour. We are grateful to Jean Bédard, James Scoates and two anonymous reviewers for helpful comments that greatly improved an earlier version of the manuscript.

REFERENCES

Ashwal, L.D., Webb, S.J. & Knoper, M.W. (2005) Magmatic stratigraphy in the Bushveld Northern Lobe: continuous geophysical and mineralogical data from the 2950m Bellevue drillcore. *South African Journal of Geology*, **108**: 199-232.

Becke, F. (1911) Uber die Ausbildung der Zwillingskristalle. *Fortschritte der Mineralogie, Kristallographie und Petrographie*, **1**: 68–85.

Bédard, J.H., Marsh, B.D., Hersum, T.G., Naslund, H.R. & Mukasa, S.B. (2007) Large-scale mechanical redistribution of orthopyroxene and plagioclase in the Basement Sill, Ferrar Dolerites, McMurdo Dry Valleys, Antarctica: petrological, mineral-chemical and field evidence for channelised movement of crystals and melt. *Journal of Petrology*, **48**: 2289-2326.

Bird, D.K., Rogers, R.D. & Manning, C.E. (1986) Mineralised fracture systems of the Skaergaard intrusion, East Greenland. *Meddelelser om Grønland, Geoscience*, **16**: 68 pp.

Bollingberg, K. (1995) Textural and chemical evolution of the Fe-Ti oxide minerals during late- and post-magmatic cooling of the Skaergaard intrusion, East Greenland. *Unpublished PhD thesis*, University of Copenhagen.

Holness, M.B. (2010) Decoding dihedral angles in melt-bearing and solidified rocks. *Journal of the Virtual Explorer*, **35**: 3.

Holness, M.B. (2015) Plagioclase growth rates control three-grain junction geometry in dolerites and gabbros. *Journal of Petrology*, **56**: 2117-2144.

Holness, M.B., Nielsen, T.F.D. & Tegner, C. (2007a) Textural maturity of cumulates: a record of chamber filling, liquidus assemblage, cooling rate and large-scale convection in mafic layered intrusions. *Journal of Petrology*, **48**: 141-157.

Holness, M.B., Tegner, C., Nielsen, T.F.D., Stripp, G., & Morse, S.A. (2007b) A textural record of solidification and cooling in the Skaergaard Intrusion, East Greenland. *Journal of Petrology*, **48**: 2359-2377.

Holness, M.B., Stripp, G., Humphreys, M.C.S., Veksler, I.V., Nielsen, T.F.D. & Tegner, C. (2011) Silicate liquid immiscibility within the crystal mush: late-stage magmatic microstructures in the Skaergaard intrusion, East Greenland. *Journal of Petrology*, **52**: 175-222.

Holness, M.B., Humphreys, M.C.S., Sides, R., Helz, R.T. & Tegner, C. (2012a) Toward an understanding of disequilibrium dihedral angles in mafic rocks. *Journal of Geophysical Research*, **117**: B06207.

Holness, M.B., Richardson, C. & Helz, R.T. (2012b) Disequilibrium dihedral angles in dolerite sills: a new proxy for cooling rate. *Geology*, **40**: 795-798.

Holness, M.B., Namur, O. & Cawthorn, R.G. (2013) Disequilibrium dihedral angles in layered intrusions: a microstructural record of fractionation. *Journal of Petrology*, **54**: 2.067-2093

Holness, M.B., Tegner, C., Namur, O. and Pilbeam, L. (2015) The earliest history of the Skaergaard magma chamber: a textural and geochemical study of the Cambridge drill core. *Journal of Petrology*, **56**: 1199-1227.

Holness, M.B., Cawthorn, R.G. & Roberts, J. (2017c) The thickness of the crystal mush on the floor of the Bushveld magma chamber. *Contributions to Mineralogy and Petrology*, **172**: 102.

Holness, M.B., Farr, R. & Neufeld, J.A. (2017d) Crystal setting and convection in the Shiant Isles Main Sill. *Contributions to Mineralogy and Petrology*, **172**: 7. Doi 10.1007/s00410-016-1325-x.

Holness, M.B., Neufeld, J.A., Gilbert, A.J., & Macdonald, R. (2017b) Orientation of tabular mafic intrusions controls convective vigour and crystallisation style. *Journal of Petrology*, **58**: 2035-2053.

Holness, M.B., Tegner, C., Nielsen, T.F.D. & Charlier, B. (2017a) The thickness of the mushy layer on the floor of the Skaergaard magma chamber at apatite saturation. *Journal of Petrology*, **58**: 909-932.

Holness, M.B., Vukmanovic, Z. & Mariani, E. (2017e) Assessing the role of compaction in the formation of adcumulates: a microstructural perspective. *Journal of Petrology*, **58**: 643-674.

Holness, M.B., Stock, M.J. & Geist, D. (2019) Magma chambers versus mush zones: constraining the architecture of sub-volcanic plumbing systms from microstructural analysis of crystalline enclaves. *Philosophical Transactions of the Royal Society*, **A377**: 20180006.

Holness, M.B., Morris, C., Vukmanovic, Z. & Morgan, D.J. (2020) Insights into magma chamber processes from the relationship between fabric and grain shape in troctolitic cumulates. *Frontiers in Earth Science*, **8**: 352. Doi:10.3389/feart.2020.00352.

Hoover, J.D. (1989a) Petrology of the Marginal Border Series of the Skaergaard Intrusion. *Journal of Petrology*, **30**: 399-439.

Hoover, J.D. (1989b) The chilled marginal gabbro and other contact rocks of the Skaergaard Intrusion. *Journal of Petrology*, **30**, 441-476.

Humphreys, M.C.S. (2011) Silicate liquid immiscibility within the crystal mush: evidence from Ti in plagioclase from the Skaergaard intrusion. *Journal of Petrology*, **52**: 147-174.

Humphreys, M.C.S. & Holness, M.B. (2010) Melt-rich segregations in the Skaergaard Marginal Border Series: tearing of a vertical silicate mush. *Lithos*, **119**: 181-192.

Irvine, T.N. (1970) Heat transfer during solidification of layered intrusions. I. sheets and sills. *Canadian Journal of Earth Sciences*, **7**: 1031-1061.

Irvine, T.N. (1980) Magmatic density currents and cumulus processes. *American Journal of Science*, **280-A**: 1-58.

Irvine, T.N., Andersen, J.C. Ø. & Brooks, C.K. (1998) Included blocks (and blocks within blocks) in the Skaergaard intrusion: geological relations and the origins of rhythmic modally graded layers. *Geological Society of America Bulletin*, **110**: 1398-1447.

Kato, H. & Cahoon, J.R. (1985) Heterogeneous nucleation model of twinned crystal growth from the melt. *Metallurgical Transactions*, **16A**: 690-692.

Kays, M.A. & McBirney, A.R. (1982) Origin of picritic blocks in the Marginal Border Group of the Skaergaard Intrusion, East Greenland. *Geochemica et Cosmochimica Acta*, **46**: 23-30.

Kays, M.A., McBirney, A.R. & Goles, G.G. (1981) Xenoliths of gneisses and the conformable, clot-like granophyres in the Marginal Border Group, Skaergaard Intrusion, East Greenland. *Contributions to Mineralogy and Petrology*, **76**, 265-284.

Keevil, H.A., Namur, O. & Holness, M.B. (2020) Microstructures and late-stage magmatic processes in layered mafic intrusions: symplectites from the Sept Iles Intrusion, Quebec, Canada. *Journal of Petrology*, **61**: egaa071. doi: 10.1093/petrology/egaa071.

Kitamura, M., Hosoya, S. & Sunagawa, I. (1979) Re-investigation of the re-entrant corner effect in twinned crystals. *Journal of Crystal Growth*, **47**: 93-99.

Larsen, R.B. & Brooks, C.K. (1994) Origin and evolution of gabbroic pegmatite in the Skaergaard intrusion, East Greenland. *Journal of Petrology*, **35**: 1651-1679.

Latypov, R. (2009) Testing the validity of the petrological hypothesis 'no phenocrysts, no post-emplacement differentiation'. *Journal of Petrology*, **50**: 1047-1069.

Latypov, R., Morse, T., Robins, B., Wilson, R., Cawthorn, G., Tener, C., Holness, M., Lesher, C., Barnes, S., O'Driscoll, B., Veksler, I., Higgins, M., Wilson, A., Namur, O., Chistyakova, S., Naslund, R. & Thy, P. (2015) A fundamental dispute: a discussion of "On some fundamentals of igneous petrology" by Bruce D. Marsh, Contributions to Mineralogy and Petrology (2013) 166: 665-690. *Contributions to Mineralogy and Petrology*, **169**: 20

Lee, J.W., Hwang, N.M. & Kim, D.Y. (2003) Growth morphology of perfect and twinned face-centred-cubic crystals by Monte Carlo simulation. *Journal of Crystal Growth*, **250**: 538-545.

Maaløe, S. (1976) Zoned plagioclase of the Skaergaard Intrusion, East Greenland. *Journal of Petrology*, **17**: 398-419.

Markl, G. (2005) Mullite-corundum-spinel-cordierite-plagioclase xenoliths in the Skaergaard Marginal Border Group: multi-stage interaction between metasediments and basaltic magma. *Contributions to Mineralogy and Petrology*, **149**: 196-215.

Marsh, B.D. (2013) On some fundamentals of igneous petrology. *Contributions to Mineralogy and Petrology*, **166**: 665-690.

McBirney, A.R. (1989a) The Skaergaard Layered Series: I. Structure and average compositions. *Journal of Petrology*, **30**: 363-397.

McBirney, A.R. (1989b) *Geological map of the Skaergaard Intrusion, East Greenland*. Eugene, Department of Geology, University of Oregon 1:20 000.

McBirney, A.R. & Nicolas, A. (1997) The Skaergaard layered series: Part II. Dynamic layering. *Journal of Petrology*, **38**: 569-580.

McBirney, A.R. & Noyes, R.M. (1979) Crystallisation and layering of the Skaergaard Intrusion. *Journal of Petrology*, **20**: 487-554.

Morse, S. A. (1986) Convection in aid of adcumulus growth. *Journal of Petrology* **27:** 1183-1215.

Morse, S.A. (1988) Motion of crystals, solute, and heat in layered intrusions. *Canadian Mineralogist*, **26**: 209-224.

Morse, S.A. (2011) The fractional latent heat of crystallising magma. *American Mineralogist*, **96**: 682-689.

Namur, O. & Humphreys, M.C.S (2018) Trace element constraints on the differentiation and crystal mush solidification in the Skaergaard intrusion, Greenland. *Journal of Petrology*, **59**: 387-418.

Namur, O., Humphreys, M.C.S., & Holness, M.B. (2013) Lateral reactive infiltration in a vertical gabbroic crystal mush, Skaergaard Intrusion, East Greenland. *Journal of Petrology*, **54**: 985-1016.

Namur, O., Humphreys, M.C.S. & Holness, M.B. (2014) Crystallisation of interstitial liquid and latent heat buffering in solidifying gabbros: Skaergaard intrusion, Greenland. *Journal of Petrology*, **55**: 1389-1427.

Naslund, H.R. (1984) Petrology of the Upper Border Series of the Skaergaard Intrusion, *Journal of Petrology*, **25**: 185-212.

Nielsen, T.F.D. (2004) The shape and volume of the Skaergaard Intrusion, Greenland: implications for mass balance and bulk composition. *Journal of Petrology*, **45**: 507-530.

Nielsen, T.F.D., Andersen, J.C.Ø., Holness, M.B., Keiding, J.K., Rudashevsky, N.S., Rudashevsky, V.N., Salmonsen, L.P., Tegner, C. & Veksler, I.V. (2015) The Skaergaard PGE and gold deposit: the result of *in situ* fractionation, sulphide saturation, and magma chamber-scale precious metal redistribution by immiscible Fe-rich melt. *Journal of Petrology*, **56**: 1643-1676.

Nielsen, T.F.D., Rudashevsky, N.S., Rudashevsky, V.N., Weatherley, S.M. & Andersen, J.C.Ø. (2019) Elemental distributions and mineral parageneses of the Skaergaard PGE-Au mineralisation: consequences of accumulation, redistribution, and equilibration in an upward-migrating mush zone. *Journal of Petrology*, **60**: 1903-1934.

Philpotts, A.R. & Ague, J. (2009) Principles of Igneous and Metamorphic Petrology. Cambridge: Cambridge University Press. pp. 700

Riegger, O.K. & Van Vlack, L.H. (1960) Dihedral angle measurement. *Transactions of the Metallurgical Society of AIME*, **218**: 933-935.

Salmonsen, L.P. & Tegner, C. (2013) Crystallisation sequence of the Upper Border Series of the Skaergaard intrusion: revised subdivision and implications for chamber-scale magma homogeneity. *Contributions to Mineralogy and Petrology*, **165**: 1155-1171.

Stickels, C.A. & Hücke, E.E. (1964) Measurement of dihedral angles. *Transactions of the Metallurgical Sociey of the AIME,* **230**: 795-801.

Taylor, H.P., Jr., & Forester, R.W. (1979) An oxygen and hydrogen isotope study of the Skaergaard Intrusion and its country rocks: a description of a 55-m.y. old fossil hydrothermal system. *Journal of Petrology*, **20**: 355-419.

Tegner, C. (1997) Iron in plagioclase as a monitor of the differentiation of the Skaergaard intrusion. *Contributions to Mineralogy and Petrology*, **128**: 45-51.

Tegner, C., Thy, P., Holness, M.B., Jakobsen, J.K. & Lesher, C.E. (2009) Differentiation and compaction in the Skaergaard intrusion. *Journal of Petrology*, **50**: 813-840.

Upton, B.G.J. (1987) Gabbroic, syenogabroic and syenitic cumulates of the Tugtutôq Younger Giant Dyke Complex, South Greenland. In: Parsons, I. (ed.): *Origins of igneous layering*, 93-123. Dordrecht: D. Reidel.

Vernon, R.H. (1968) Microstructures of high-grade metamorphic rocks at Broken Hill, Australia. *Journal of Petrology*, **9**: 1-22.

Vukmanovic, Z., Holness, M.B., Monks, K. & Andersen, J.C. O. (2018) The Skaergaard trough layering:

sedimentation in a convecting magma chamber. *Contributions to Mineralogy and Petrology*, **173**: 43. Doi.org/10.1007/s00410-018-1466-1.

Vukmanovic, Z., Holness, M.B., Stock, M.J. & Roberts, R.J. (2019) The creation and evolution of crystal mush in the Upper Zone of the Rustenburg Layere Suite, Bushveld Complex, South Africa. *Journal of Petrology*, **60**: 1523-1542.

Wager, L.R. & Brown, G.M. (1968) *Layered Igneous Rocks*. Freeman, San Francisco. pp.588

Wager, L.R. & Deer, W.A. (1939) Geological investigations in East Greenland. Part III. The petrology of the Skaergaard intrusion, Kangerdlussuaq, East Greenland. *Meddelelser om Grønland*: **105**.

Weatherley, S., Andersen, J.C.Ø., Holness, M.B., Dyck, B.J., Nicoli, G., & Honour, V.C. (2018) Combined 'sedimentary' and in-situ origin for magmatic Fe-Ti-V deposits: new insights from the Skaergaard Intrusion, East Greenland. *33rd Nordic Geological Winter Meeting*, https://2dgf.dk/foreningen/33rd-nordic-geological-winter-meeting/ngwm-2018-abstracts/1-igneous-rocks-and-processes/#5

White, C.M., Geist, D.J., Frost, C.D. & Verwoerd, W.J. (1989) Petrology of the Vandfaldsdalen microdike, Skaergaard region, East Greenland. *Journal of Petrology*, **30**: 271-298.

Wieser, P.E., Vukmanovic, Z., Kilian, R., Ringe, E., Holness, M.B., Maclennan, J. & Edmonds, M. (2019) To sink, swim, twin, or nucleate: a critical appraisal of crystal aggregation processes. *Geology*, **47**: 948-952.

Yuan, Q., Namur, O., Fischer, L.A., Roberts, R.J., Lü, X & Charlier, B. (2017) Pulses of plagioclase-laden magmas and stratigraphic evolution in the Upper Zone of the Bushveld Complex, South Africa. *Journal of Petrology*, **58**: 1619-1644.

FIGURE CAPTIONS

Figure 1 – Simplified geological map of the Skaergaard Intrusion, after McBirney (1989b), showing the position of the 9 sample traverses, together with the position of the collars of the Cambridge, 90-10 and 90-22 drill cores. The asterisks between the inner end of Traverse 8 on the Skaergaard Peninsula and the 90-10 drill core show the position of surface samples collected along strike in UZb. The large arrows show the dip of the contact (from Wager & Deer, 1939; Wager & Brown, 1968; Irvine *et al.,* 1998). The dashed line in the south of Kraemer Ø shows the trace of a pre-existing (or syn-magmatic) fault, assumed vertical (Nielsen, 2004).

Figure 2 – Schematic of the mineralogical subdivisions of the MBS, together with the stratigraphic position of the traverses, after Hoover (1989a). The clustering of xenoliths at the wall between Traverses 3 and 4 occurs to the south of a faulted off-set of the contact. The unconformity between the gneissic basement and the overlying Palaeogene plateau basalts (separated by a thin layer of sediments) outcrops on Mellemø: the contact is shallow where it crosses this unconformity, creating a step of unknown width. Note that the first appearance of LZc* on the western margin occurs on the Mini-Peninsula, rather than structurally lower on Ivnarmiut as suggested by Hoover (1989a). There is likely to be very little LZc* on the Skaergaard Peninsula: the boundary between LZc* and MZ* is thus drawn as a dashed line. The width of UZa* on the Skaergaard Peninsula is a few tens of metres, much less than the thickness suggested by Hoover (1989a).

Figure 3 – The Wavy Pyroxene Rock in the outer part of the MBS on north Kraemer Ø. (a) Close to the contact, the Wavy Pyroxene Rock is distinguished by the presence of abundant, penny-shaped coarse-grained pockets of late-stage liquid which consistently dip towards the intrusion contact. (b) The morphology of the pockets of late-stage liquid changes with increasing distance from the contact: they become more diffuse, larger and more irregular in shape, linked to the decreasing cohesion and strength of the mush as it became thicker with time (Humphreys & Holness, 2010). Here they are commonly concave-upwards in cross-section, with an upper pale, plagioclase-rich region, and a lower melanocratic rim.

Figure 4 – The inner parts of the MBS are characterised by vertical or steeply-dipping modally-graded layers, the morphology of which evolves with increasing distance from the contact. (a) The outermost bands are either planar or slightly colloform, with cusps pointing towards the contact. The cuspate morphology becomes more developed with increasing distance from the contact: Mini-Peninsula. (b) in the most evolved parts of the MBS, the colloform bands are so deeply cuspate that the ends of the cusps are extremely well-developed and clearly visible as separate, mafic entities when viewed from above. (c) in longitudinal cross-section these most extreme form of the colloform bands are visible as trough-like structures dipping steeply into the intrusion. Examples are arrowed. Both (b) and (c) from the inner part of the MBS on Ivnarmiut, with hammer for scale.

Figure 5 – The cross-bedded belt. (a) Uttental Plateau. The cross-bedded belt is notable for abundant small angular unconformities in thinly layered cumulates, with many syn-magmatic shear zones and normal faults with throws down into the intrusion. Note the almost vertical vein of leucocratic material near the rifle, denoting migration of late-stage liquid through the cohesive mush along one of these syn-magmatic fractures that offset material on either side (unusually, this one appears to be a reverse fault). The upper part of this offset is marked by arrows. (b) The boundary between the Layered Series and the MBS is a well-defined planar surface on the northern part of Kraemer Ø (arrowed and marked by a dashed line), separating coarse-grained almost featureless MBS gabbro on the right from relatively melanocratic and weakly modally banded Layered Series on the left (orientation of layers shown by white lines). Field of view is ~4m high.

Figure 6 – The boundary between the Layered Series and the MBS on the southern part of Ivnarmiut. (a) Well-defined modal layering in the Layered Series (on the left, with an indicative dotted line showing the layering) overlies the inwards-dipping edge of the relatively leucocratic MBS. The contact is marked by a melanocratic band, seen in top view in (b). This band is up to some tens of cm wide, with sharply-defined inner and outer margins (shown by dotted lines). Compass-clinometer for scale. (c) View looking down on the outcrop shown from the side in (a), with the Layered Series at the top of the image, divided from the MBS at the bottom by the melanocratic band (the outer margin of which is shown by the dotted line). Note

the well-defined modal colloform bands in the MBS (two are marked by asterisks) that are truncated by the oxide-rich layer defining the boundary with the Layered Series. The compass-clinometer can be seen about a metre to the right of the left-hand arrow, on the contact.

Figure 7 – The stratigraphic variation of the median clinopyroxene-plagioclase-plagioclase dihedral angle, Θ_{cpp}, through the Skaergaard Layered Series. (a) Θ_{cpp} as a function of stratigraphic height in the standard profile of Tegner *et al*. (2009) through the central part of the intrusion, supplemented by data from the Cambridge drill core (location shown in Figure 1). The continuous line shows Θ_{cpp} as presented by Holness *et al.* (2007a), whereas the data points with 2σ uncertainties are from Holness *et al.* (2013). The upper parts of this traverse comprise the drill core 90-22 (location shown in Figure 1). (b) Details of the variation of Θ_{cpp} in the vicinity of the UZa/b boundary (from Holness *et al*., 2017a), marked by the saturation of the bulk liquid in apatite, as observed in the drill core 90-10 (see Figure 1 for location). The vertical grey bars show the location of dolerite dykes in the core. Note the continuous high values of Θ_{cpp} in UZa, in contrast to the steadily decreasing values in the standard section: the latter are associated with macro-dolerite, whereas macro-dolerite is only present locally in UZb in core 90-10. The mush thickness is given by the stratigraphic distance between the step-change in Θ_{cpp} triggered by the saturation of the bulk magma in apatite, and the first appearance of apatite primocrysts in the stratigraphy. In this part of the floor, the mush was ~100m thick at the moment the bulk liquid became saturated in apatite (Holness *et al.,* 2017a).

Figure 8 – Photomicrographs of MBS gabbros, with contrasting examples of the outermost Layered Series. Scale bars in all images are 1mm long. All figures under crossed polars, except (f) and (g) which are in plane polarised light. Abbreviations: ol – olivine; px – pyroxene; ap – apatite. (a) Sample SP59, 17.5m from the contact on the Skaergaard Peninsula, LZa*. The plagioclase-plagioclase grain boundaries are non-planar, and not all parallel to expected growth faces for the grains on either side. Note the abundance of included grains of plagioclase within larger plagioclase grains. This image also contains anhedral grains of olivine and pyroxene, with an interstitial habit. (b) Sample SP61, from a few metres from the contact on the Skaergaard Peninsula, LZa*. Olivine primocrysts are commonly anhedral, with irregular overgrowths (seen here as apparently disconnected grains in optical continuity) from interstitial liquid. (c) Sample KR01/44, 105m from the contact in the centre of Kraemer Ø, LZa*. Subhedral olivine primocrysts form clusters which are joined on likely olivine growth faces, denoting growth as individual crystals before cluster formation. (d) Sample KR01/17, 158m from the contact in the centre of Kraemer Ø, LZb*. Augite primocrysts are anhedral or subhedral, forming compact grains with no inclusions. (e) Sample SP63, 294m from the contact on the Skaergaard Peninsula, LZb*. Augite here forms euhedral primocrysts, generally with a simple (100) twin. Most grains depicted are sectioned perpendicular to the *z*-axis, so their common elongation along [001] is not visible. (f) Sample KR03/24, 332m from the contact in the south of Kraemer Ø, MZ. Although this sample is from the outermost part of the Layered Series, it illustrates well the euhedral shape of the Fe-Ti oxide primocrysts, with elongate prisms of ilmenite and octahedra of magnetite, associated with abundant augite. (g) Sample SP29, 594m from the contact on the Skaergaard Peninsula, UZb*. The abundant apatite primocrysts are euhedral. Note the branched nature of the Fe-Ti oxides, intimately intergrown with pyroxene and olivine – these form by the solidification of an exsolved immiscible Fe-rich liquid. The Si-rich conjugate solidifies as granophyre (arrowed). (h) Sample SP70, 749m from the contact on the Skaergaard Peninsula, UZb. The primocrysts of olivine, pyroxene and plagioclase are predominantly euhedral, signifying accumulation after a period of growth isolated within a liquid-rich environment. Granophyre (arrowed) fills pores bounded by plagioclase grains. The asterisk marks the single example within this image of a grain with evidence of intra-crystalline plasticity.

Figure 9 – Photomicrographs of the melanocratic band separating the MBS from the outermost Layered Series on the south of Ivnamuit (Figure 6b). All images except (a) are taken under crossed polars. (a) Thin section scan showing the microstructure formed of isolated euhedral to subhedral grains of augite (px), plagioclase (pl) and olivine. Note the weak preferred orientation of the more elongate grains. Scale bar is 4mm long. (b) Isolated grains of the primocryst phases augite, olivine (ol), plagioclase and Fe-Ti oxides. Scale bar is 0.5 mm long. (c) Twinned augite primocryst with euhedral plagioclase. Note the lattice distortion in the plagioclase grain on the right and the interstitial shape of the oxide grains. Note also the polygonal fine-grained plagioclase separating the two larger plagioclase grains (arrowed). Scale bar is 0.5 mm long. (d) Large plagioclase grains, one of which shows evidence of lattice distortion, separated by polycrystalline bands of granular plagioclase (arrowed). Scale bar is 0.5 mm long. (e) Close view of the polycrystalline plagioclase bands that separate the larger primocrysts. Scale bar is 0.5 mm long. (f) The polycrystalline granular-textured plagioclase-rich band (arrowed) surrounding this large plagioclase primocryst also contains grains of Fe-Ti oxides. Scale bar is 0.5 mm long.

Figure 10 – The values of Θ_{cpp} for each of the nine sample traverses, keyed into their location in the MBS (inset map modified after Hoover (1989a): the position of the Vandvaldsdalen traverse on the east margin is not shown). See Supplementary Appendix A for the complete dataset. The mineralogical subdivisions within each traverse are shown, and the thickness and position of the transition into the outer margin of the Layered Series is indicated by a grey band (the inner edge of the MBS is shown as a line on the left side of the grey band). The two traverses across the Mini-Peninsula are superimposed, with the correlation based on the placement of the single sample of LZc* in the shorter traverse (data points marked with an open circle) at the well-defined boundary between LZb* and MZ* on the detailed traverse (data points marked with a black circle). The position of the outermost colloform band in each traverse is shown by a grey dashed line, and the position of the step-changes in Θ_{cpp} are shown by arrows at the base of each plot.

Figure 11 – Spatial variation of selected components of the bulk rock composition across the MBS in the north of Kraemer Ø. The subdivisions and the cross-bedded belt are as shown in Figure 10. See Supplementary Appendix B for the complete dataset.

Figure 12 – Spatial variation of selected components of the bulk rock composition across the MBS on Ivnarmiut. The plagioclase composition is that calculated for normative plagioclase. The subdivisions and the cross-bedded belt are as shown in Figure 10. The grey data points for Mg# and normative plagioclase composition are those for the equivalent Layered Series subdivisions, with the data from Tegner *et al.* (2009) stretched so that the subdivision boundaries occur in the same place: the Tegner *et al*. (2009) data for LZc are not shown and the entire MZ dataset is compressed to fit the width of MZ*. See Supplementary Appendix B for the complete dataset.

Figure 13 – Spatial variation of selected components of the bulk rock composition across the MBS on the Skaergaard Peninsula. Details as for Figure 12. The entire UZa and UZb datasets of Tegner *et al*. (2009) are compressed to fit into the respective widths of UZa* and UZb*. See Supplementary Appendix B for the complete dataset.

Figure 14 – The volume fraction of late-stage intergrowths as a function of distance from the intrusion margin on the Skaergaard Peninsula (Traverse 8). The grey shaded box indicates the cross-bedded belt, with the inner edge of the MBS marked as a black line on its left margin. The locations of the UZb samples are shown in Figure 1. The furthermost two samples are from the top of the 90-10 drill core.

Figure 15 – The thickness of the crystal mush on the Skaergaard chamber walls as a function of overall thickness of the MBS. The overall thickness of the MBS at each of the moments marked by a step-change in Θ_{cpp} is taken as the distance from the intrusion's margin to the inner edge of the wall mush marked by the associated arrival of the new primocryst phase. The markers p, o and a denote estimates of mush thickness derived from the steps associated with pyroxene-in, oxide-in and apatite-in, respectively.

Table 1 – ranges of Θ_{cpp} observed in the sub-divisions of the MBS (Figure 10), with the equivalent values in the Layered Series for comparison.

Location	**LZa***	**LZb***	**MZ*/UZa***
Uttental Plateau	87-89	-	-
Vandvaldsdalen	86-87	93-95	-
North Kraemer	84-87	90-91	-
Central Kraemer	83-85	90-92	-
South Kraemer	84-86	91-93	99-100
Ivnarmiut	85-86	90-91	94-96.5
Mini-Peninsula	-	89-91	95-97
Skaergaard Peninsula	81-84	85-87	91-92
Equivalent Layered Series	*82-85*	*95-100*	*100*

Figure 1

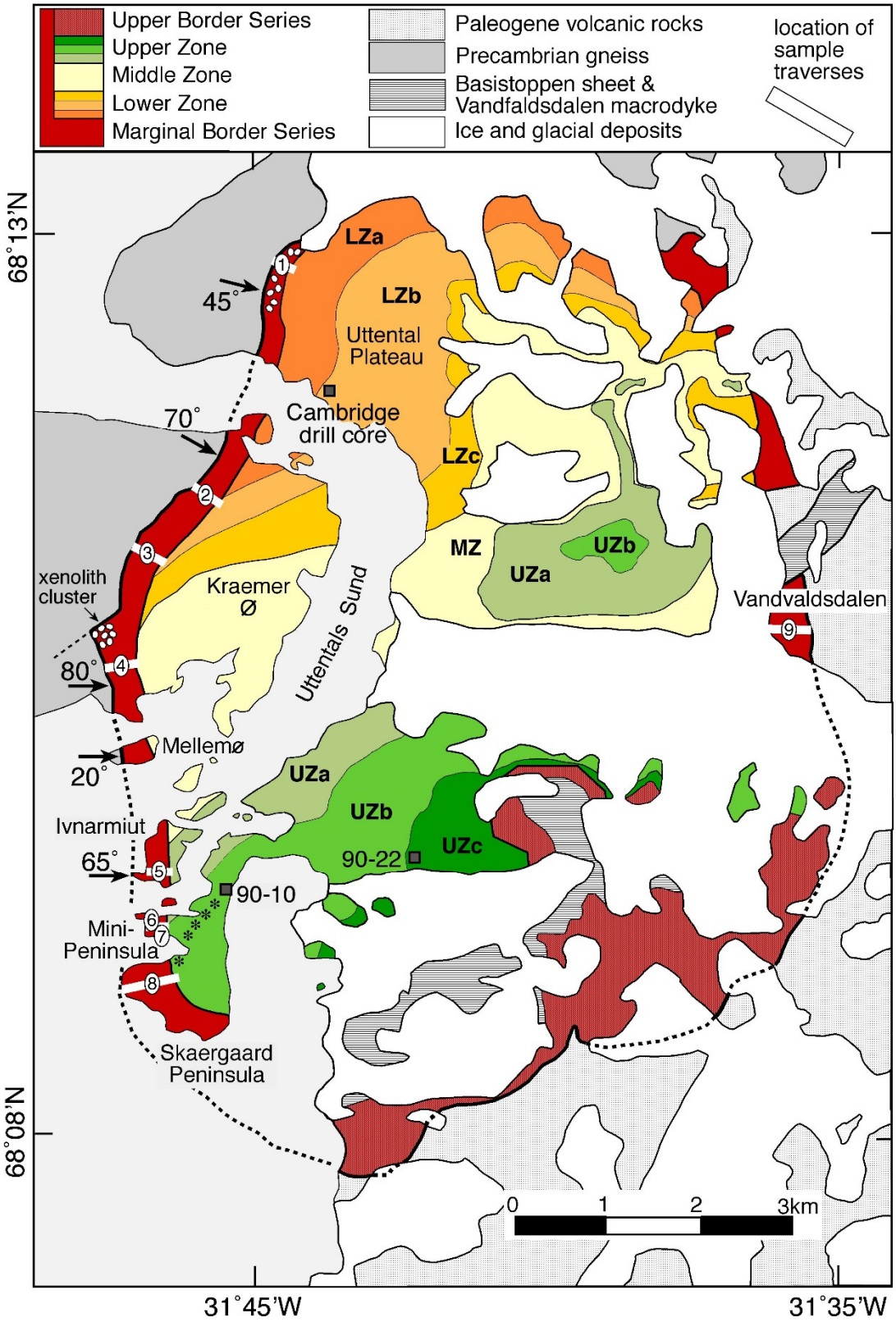
Upper Border Series
Upper Zone
Middle Zone
Lower Zone
Marginal Border Series
Paleogene volcanic rocks
Precambrian gneiss
Basistoppen sheet & Vandfaldsdalen macrodyke
Ice and glacial deposits
location of sample traverses
68°13'N
68°08'N
31°45'W
31°35'W
LZa
LZb
LZc
Uttental Plateau
Cambridge drill core
MZ
UZa
UZb
UZc
Kraemer Ø
Uttentals Sund
xenolith cluster
Vandvaldsdalen
Mellemø
Ivnarmiut
90-22
90-10
Mini-Peninsula
Skaergaard Peninsula
45°
70°
80°
20°
65°
1
2
3
4
5
6
7
8
9
0
1
2
3km

Figure 2

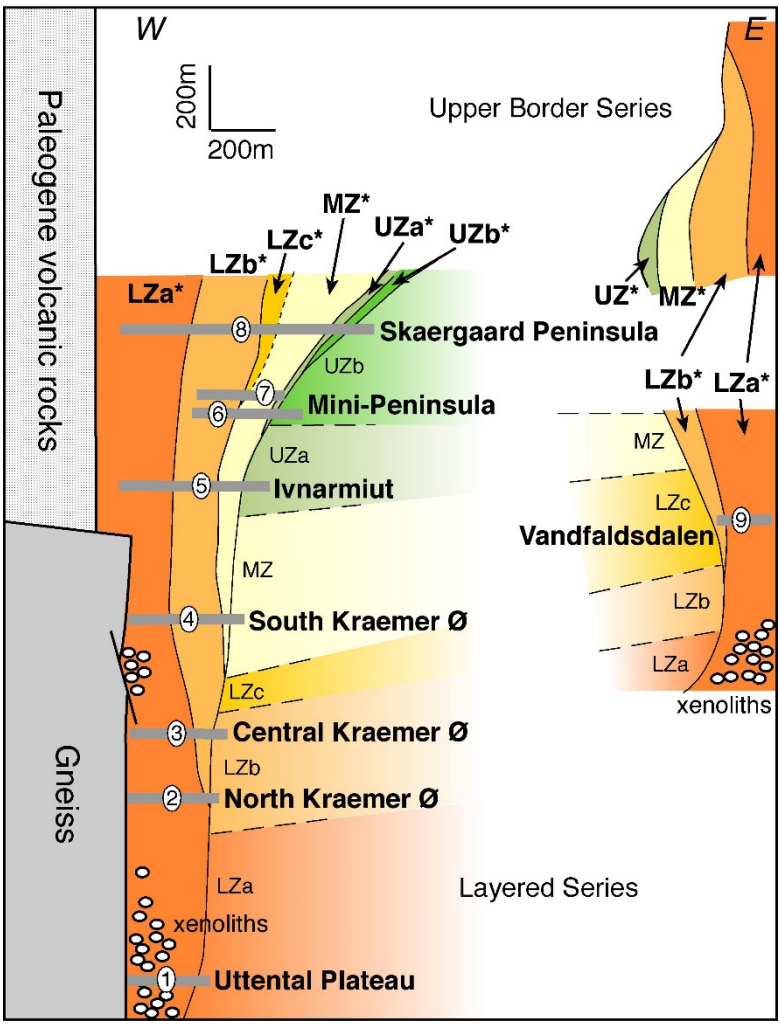
W
E
200m
200m
Upper Border Series
Paleogene volcanic rocks
Gneiss
MZ*
LZc*
UZa*
UZb*
LZb*
LZa*
UZ*
MZ*
LZb*
LZa*
8
Skaergaard Peninsula
UZb
7
6
Mini-Peninsula
UZa
5
Ivnarmiut
MZ
LZc
9
Vandfaldsdalen
MZ
LZb
LZa
xenoliths
4
South Kraemer Ø
LZc
3
Central Kraemer Ø
LZb
2
North Kraemer Ø
LZa
Layered Series
xenoliths
1
Uttental Plateau

Figure 3

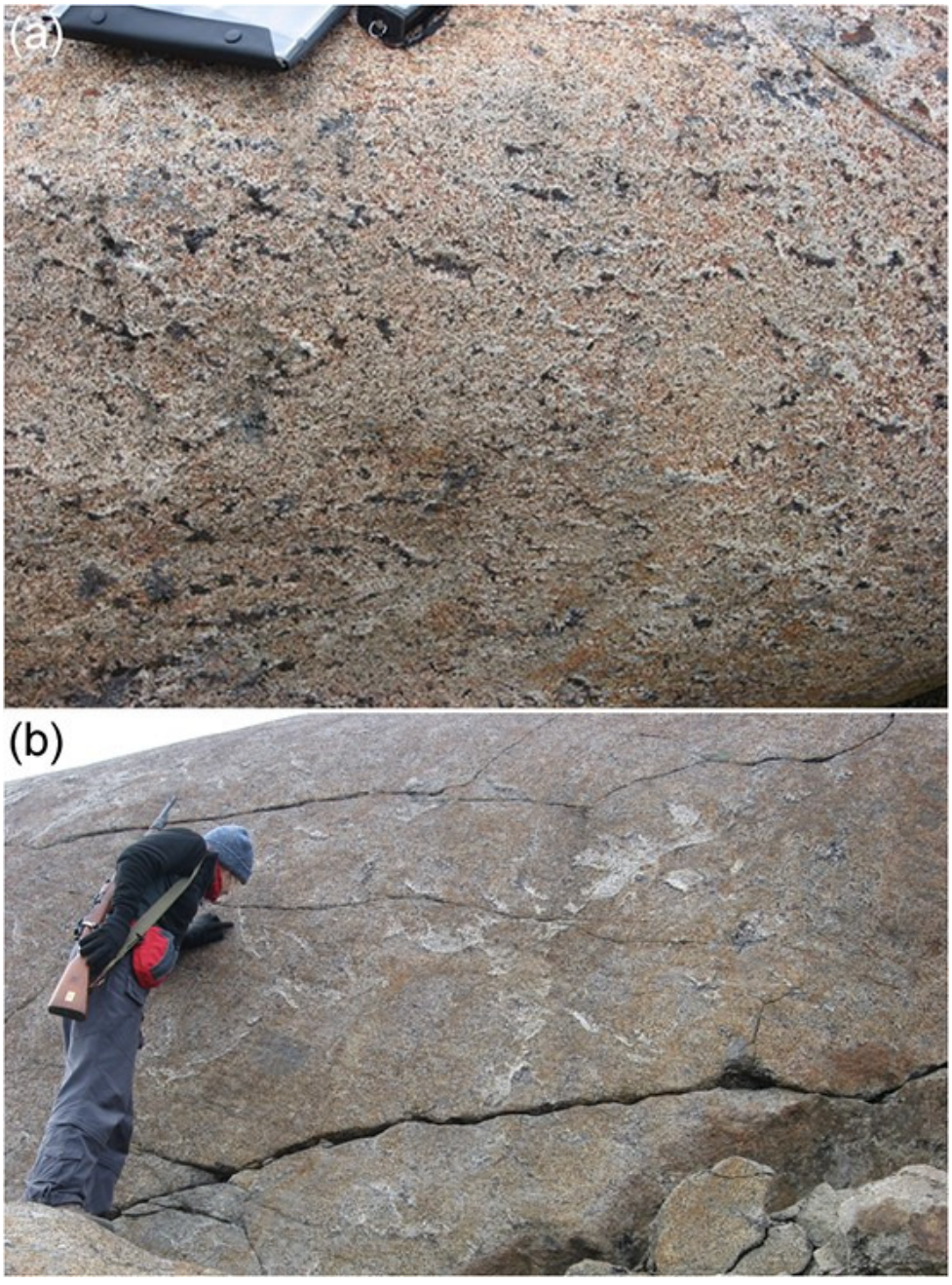

Figure 4

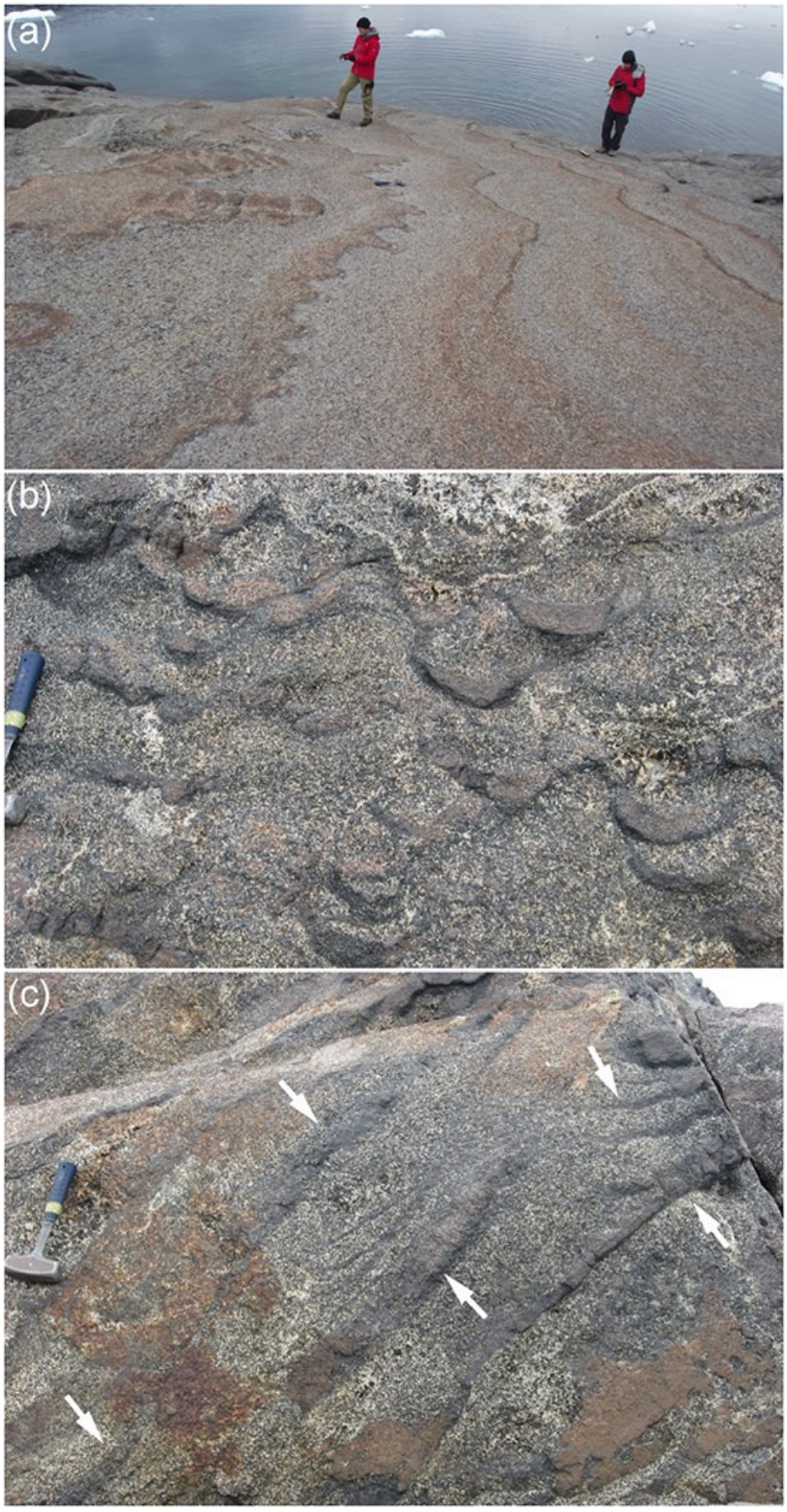

Figure 5

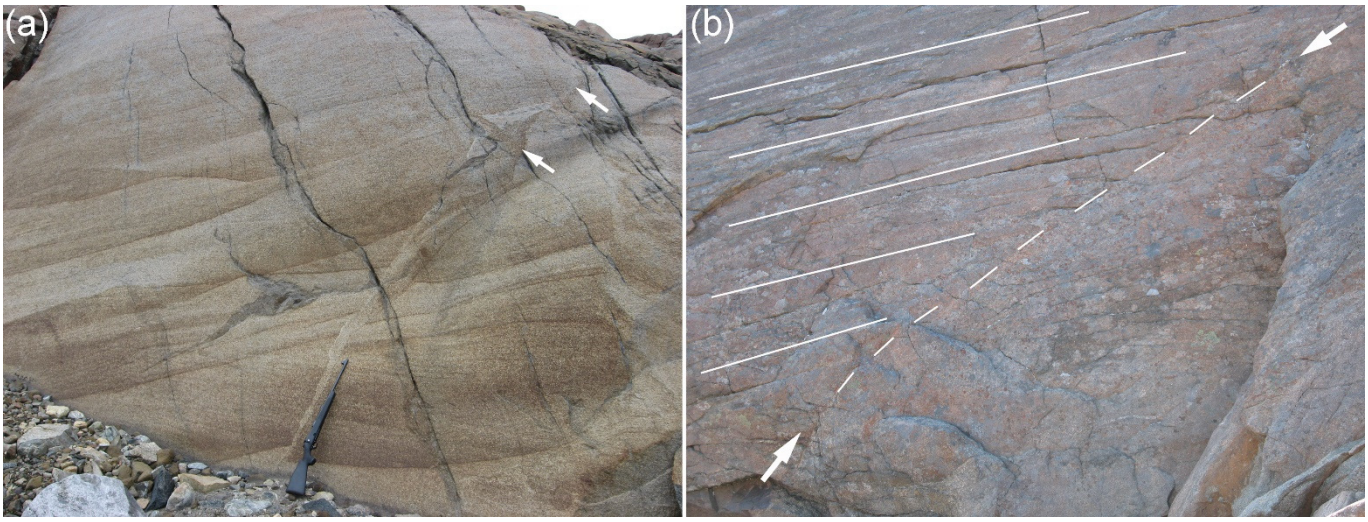

Figure 6

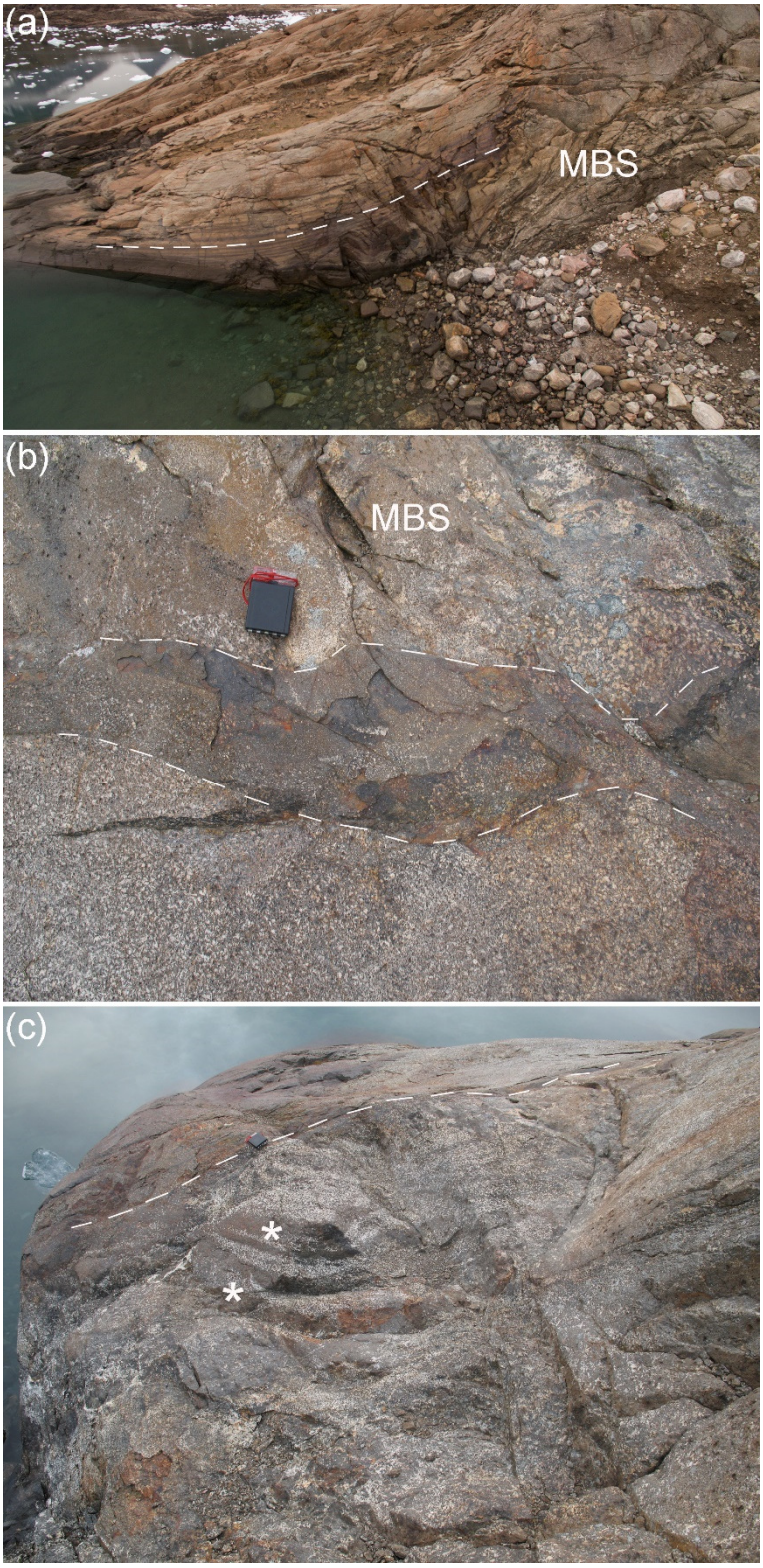

Figure 7

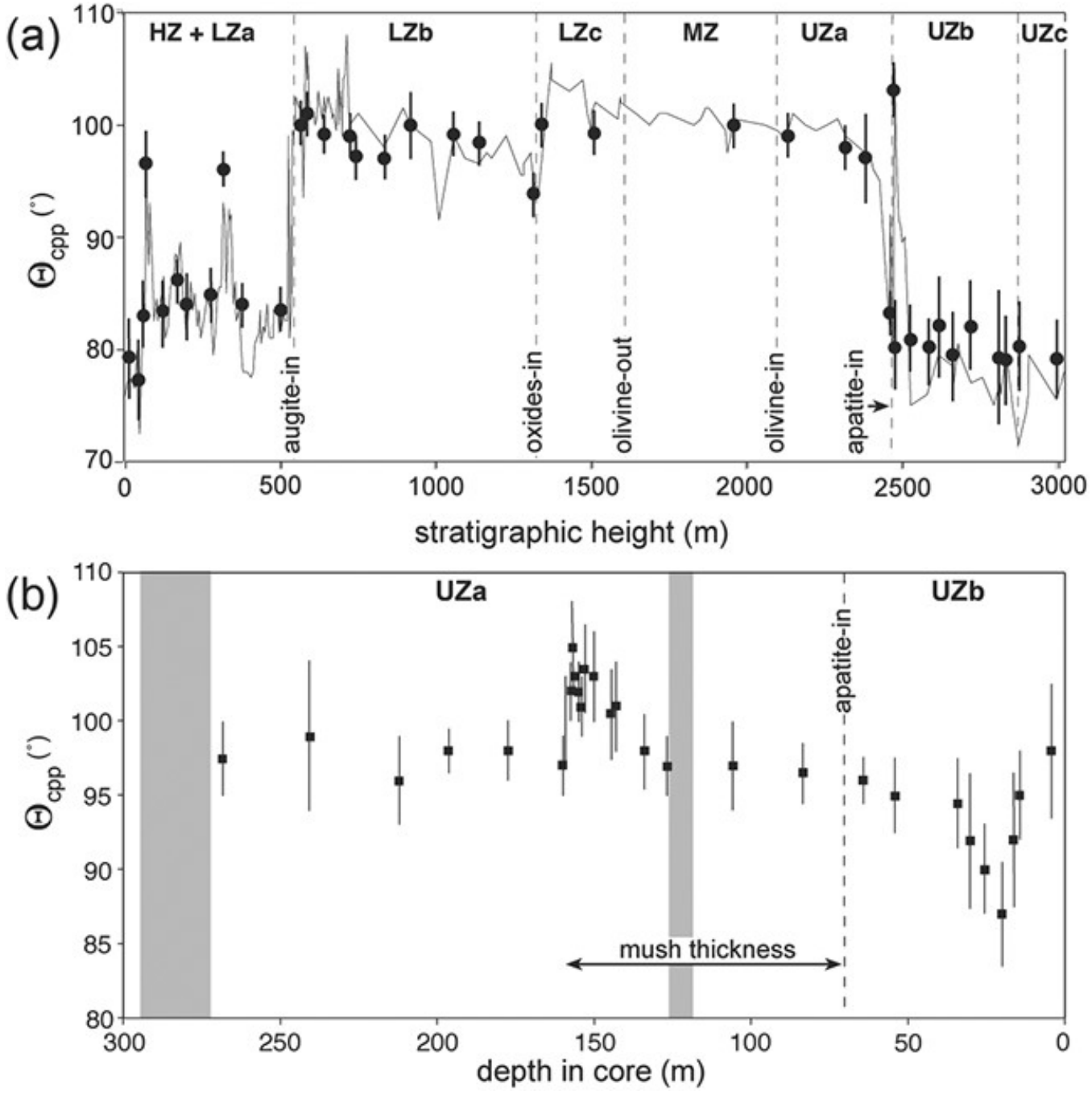
(a)
HZ + LZa
LZb
LZc
MZ
UZa
UZb
UZc
augite-in
oxides-in
olivine-out
olivine-in
apatite-in
Θcpp (°)
stratigraphic height (m)
(b)
UZa
UZb
apatite-in
mush thickness
Θcpp (°)
depth in core (m)

Figure 8

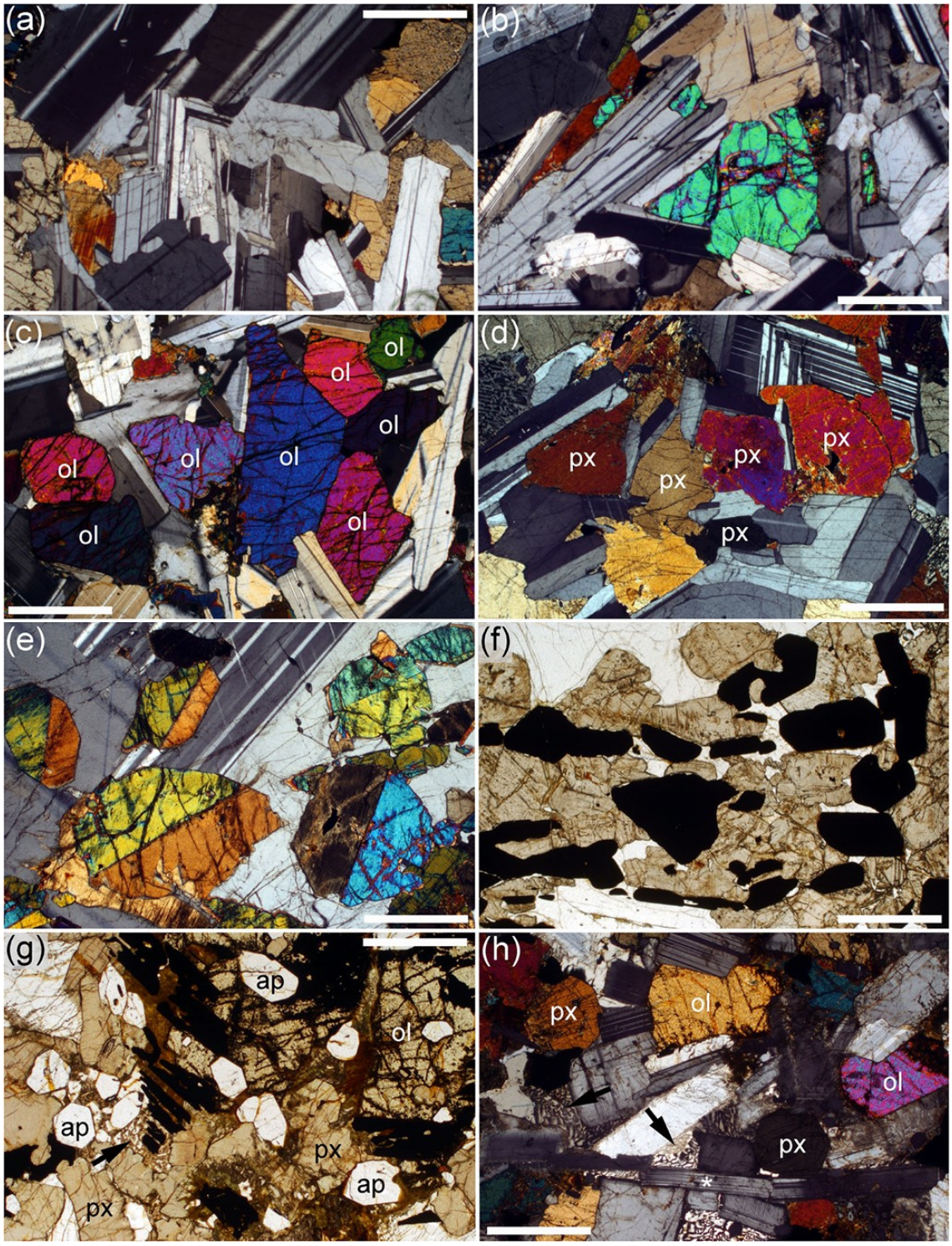
(a)
(b)
(c)
ol
ol
ol
ol
ol
ol
ol
(d)
px
px
px
px
px
(e)
(f)
(g)
ap
ol
ap
px
ap
px
(h)
px
ol
ol
px

Figure 9

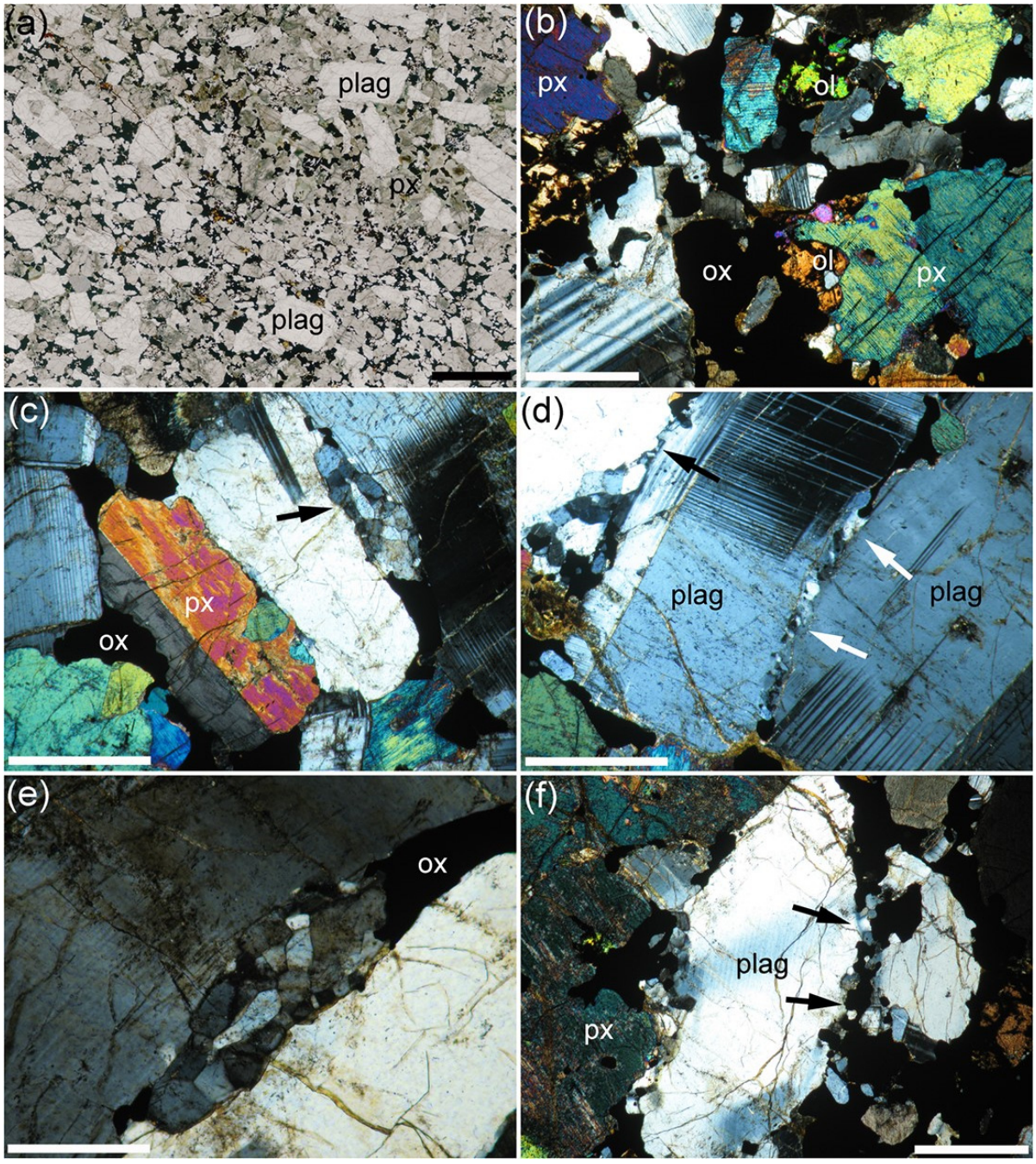

Figure 10

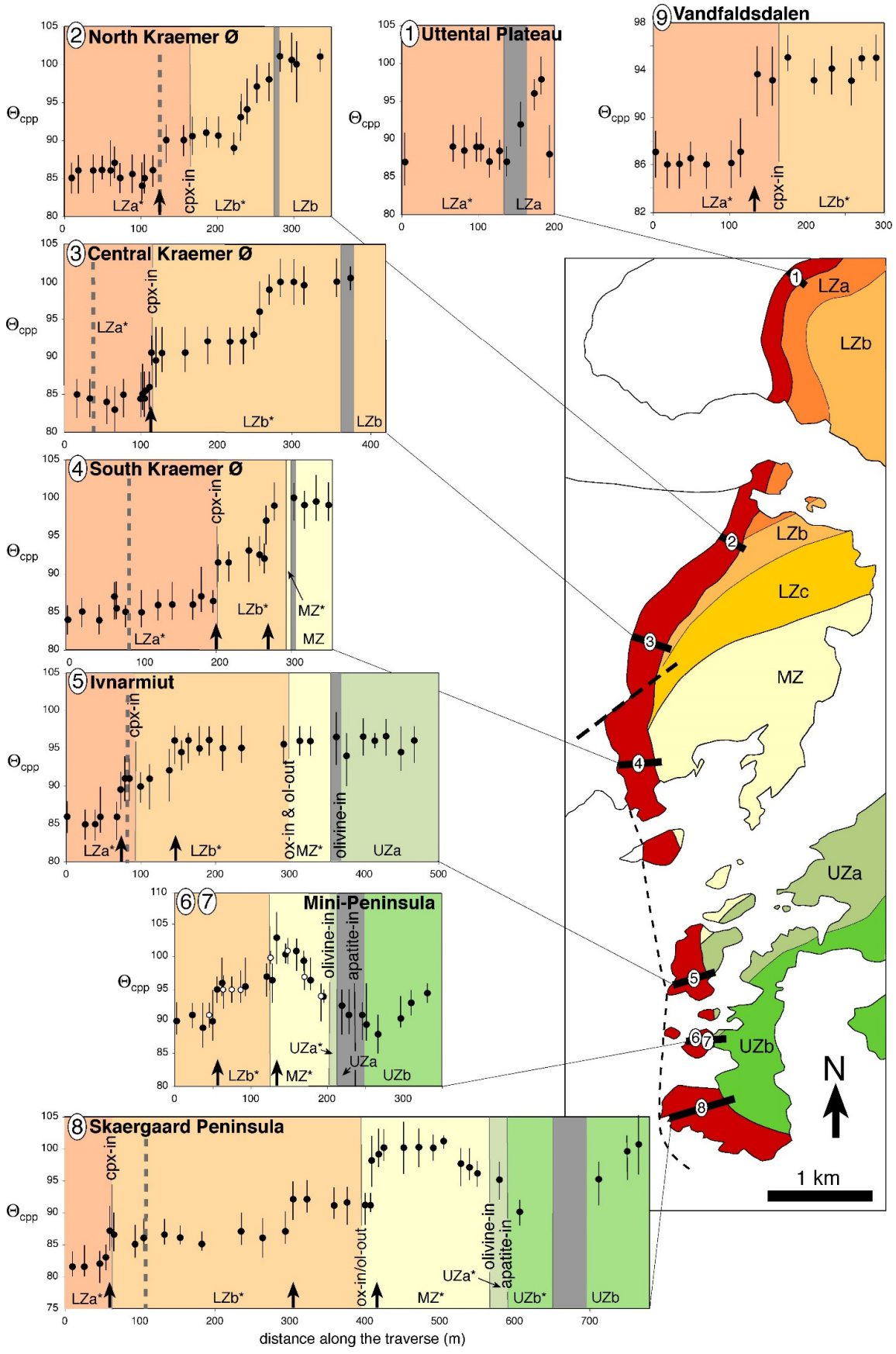
2 North Kraemer Ø
1 Uttental Plateau
9 Vandfaldsdalen
3 Central Kraemer Ø
4 South Kraemer Ø
5 Ivnarmiut
6 7 Mini-Peninsula
8 Skaergaard Peninsula
Θcpp
cpx-in
olivine-in
apatite-in
ox-in & ol-out
ox-in/ol-out
LZa*
LZb*
MZ*
UZa*
LZa
LZb
LZc
MZ
UZa
UZb
N
1 km
distance along the traverse (m)

Figure 11

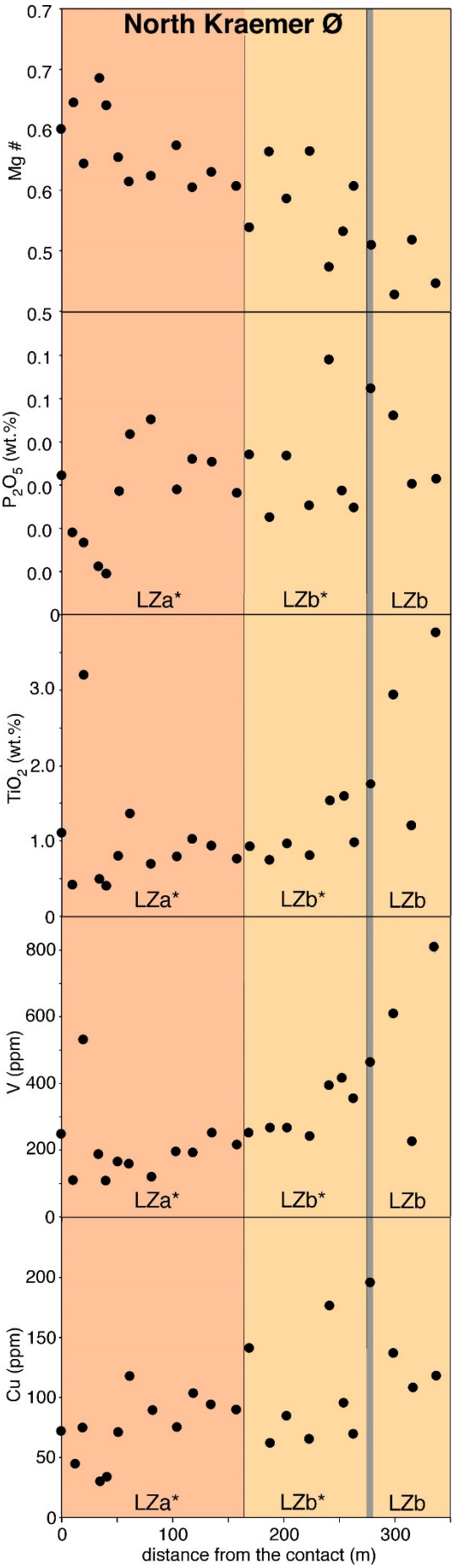
North Kraemer Ø
Mg #
0.7
0.6
0.5
P_2O_5 (wt.%)
0.1
0.0
TiO_2 (wt.%)
3.0
2.0
1.0
0
V (ppm)
800
600
400
200
Cu (ppm)
200
150
100
50
LZa*
LZb*
LZb
0
100
200
300
distance from the contact (m)

Figure 12

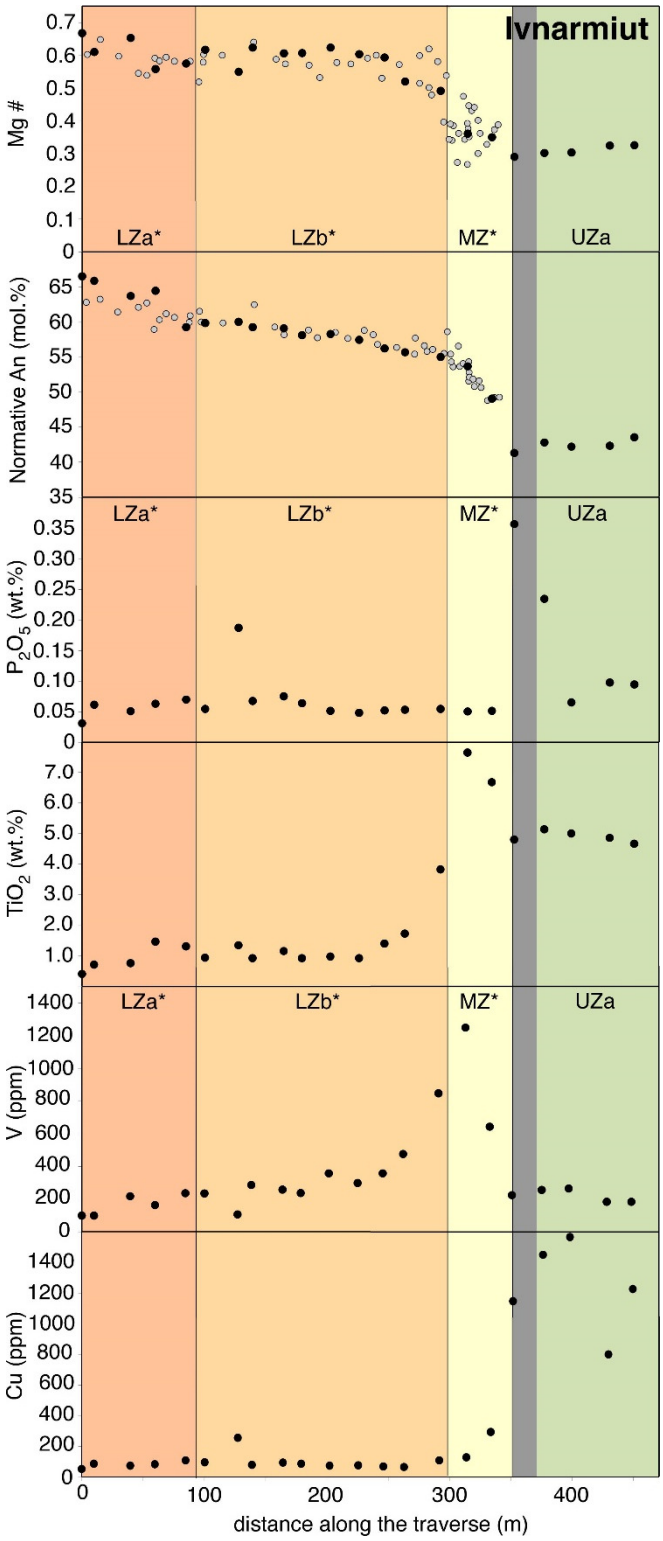
Ivnarmiut
Mg #
Normative An (mol.%)
P_2O_5 (wt.%)
TiO_2 (wt.%)
V (ppm)
Cu (ppm)
LZa*
LZb*
MZ*
UZa
distance along the traverse (m)

Figure 13

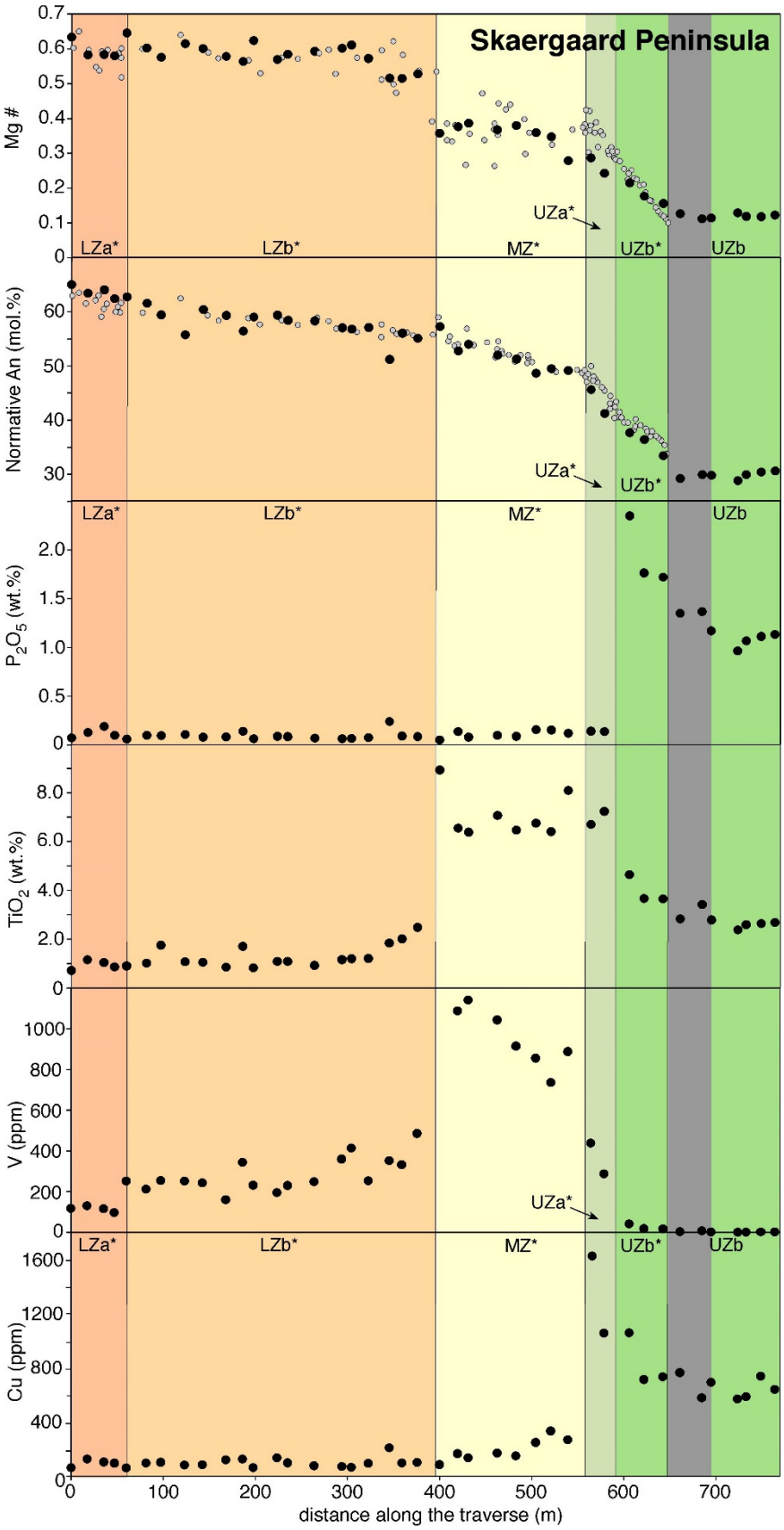
Skaergaard Peninsula
Mg #
Normative An (mol.%)
P_2O_5 (wt.%)
TiO_2 (wt.%)
V (ppm)
Cu (ppm)
LZa*
LZb*
MZ*
UZa*
UZb*
UZb
distance along the traverse (m)

Figure 14

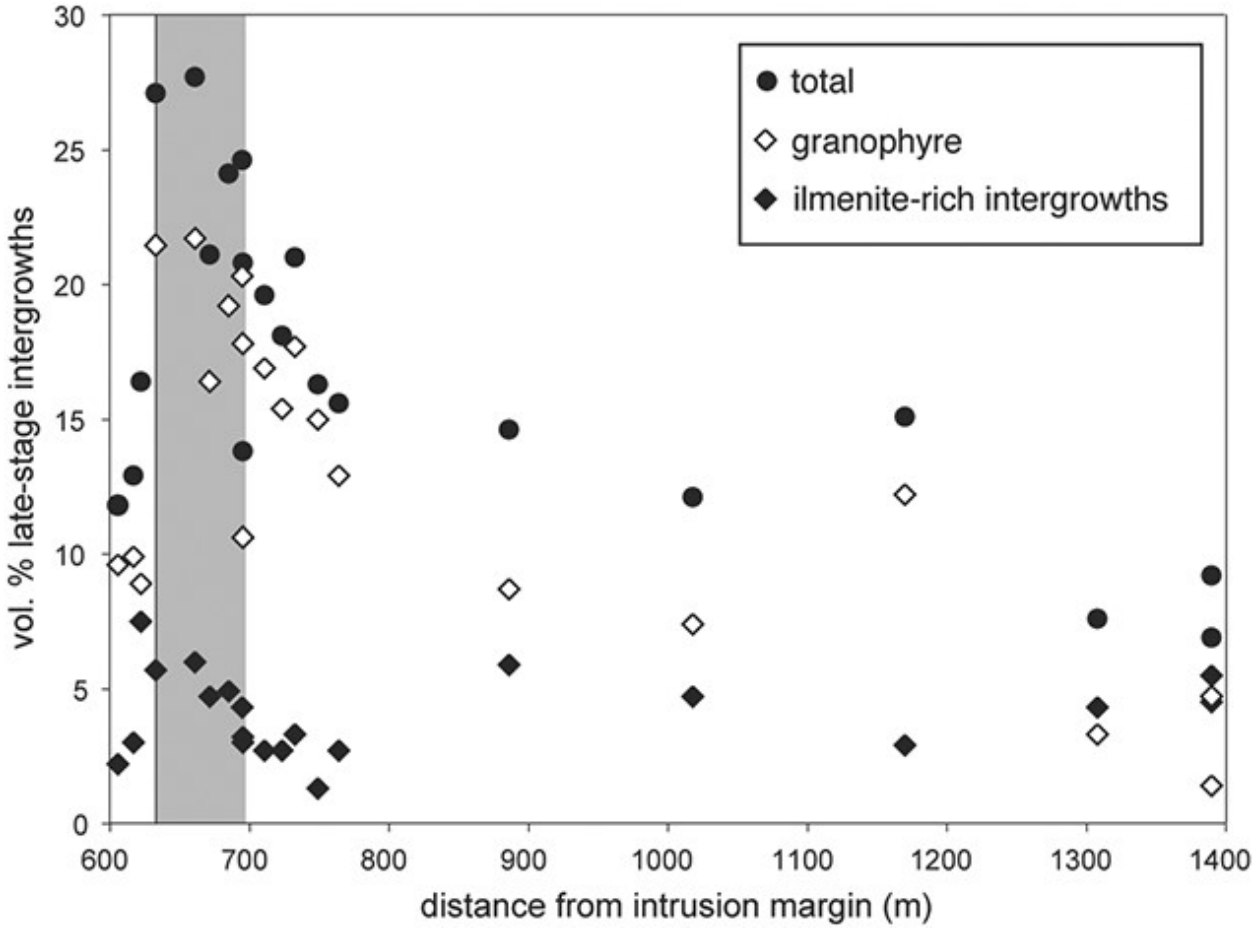
total
granophyre
ilmenite-rich intergrowths
vol. % late-stage intergrowths
distance from intrusion margin (m)
0
5
10
15
20
25
30
600
700
800
900
1000
1100
1200
1300
1400

Figure 15

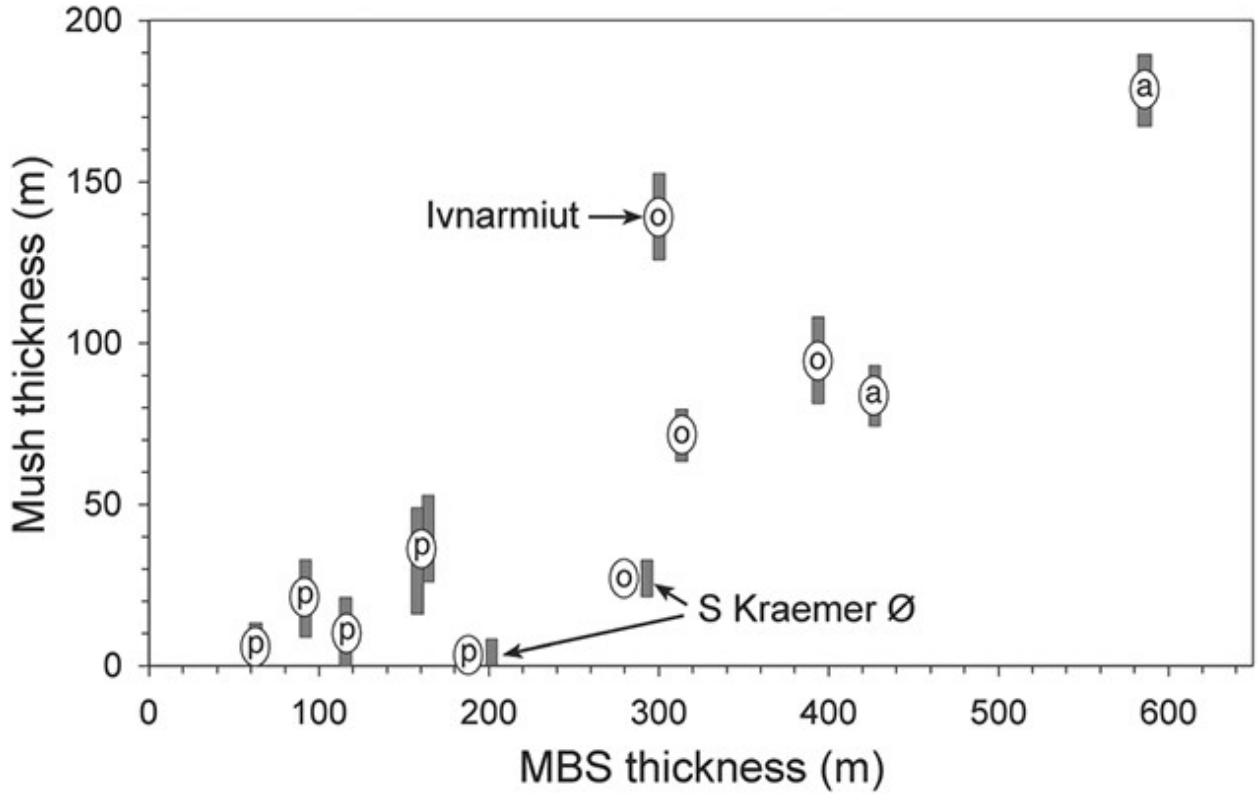
Mush thickness (m)
MBS thickness (m)
0
50
100
150
200
0
100
200
300
400
500
600
Ivnarmiut
S Kraemer Ø
p
o
a